Bachelor Thesis

Bachelor's degreee in Industrial Technology Engineering

Development of an electrical sizing tool for an offshore wind farm

June, 2019

Author: Clara Fernandez i Clemente

Director: Oriol Gomis Bellmunt

Call: 06/2019

Escola Tècnica Superior
d'Enginyeria Industrial de Barcelona

Abstract

Offshore wind power technology is still in development, therefore there is a gap for new designs in order to reduce costs and increase the efficiency. The cable size is an important factor regarding the large investments required in an offshore wind farm.

The main aim of this thesis is to optimize the cable sections for three different offshore wind farms, taking into account the costs of the cables and the costs of the energy losses. This optimization is performed through a multi-objective function and the optimum point of the Pareto front.

Firstly, the fundamentals of the project are presented, such as a brief explanation of the parts concerning an offshore wind power plant, paying special attention to the cables as are the element of study; the electric design, focusing on the cable model and the power flow analysis; the Newton-Raphson method, since is the method applied for the optimization; and the cost models for the cables and energy losses due to being the objective of minimization. Secondly, the optimization is explained and further applied for cable sizing, and the preliminary work is introduced. Thirdly, the three cases of study are presented, with the reference and optimized design respectively, and a brief discussion of the results is made. Finally, the conclusions are drawn, firstly for the results of the case study and afterward for the hole project.

Contents

List of Figures

List of Tables

List of Acronyms

AC	Alternating Current
CAPEX	Capital Expenditure
DC	Direct Current
DFIG	Doubly Fed Induction Generator
EPR	Cross-linked ethylene propylene rubber
FLH	Full Load Hours
FRC	Fully Rated Converter
HVAC	High Voltage Alternating Current
LCOE	Levilized Cost of Electricity
MOO	Multi-Objective Optimization
MVAC	Medium Voltage Alternating Current
NBI	Normal Boundary Intersection
NPV	Net Present Value
NR	Newton-Raphson
OPEX	Operational Expenditure
OWPP	Offshore Wind Power Plant
ROC	Rank order centroid
RS	Rank-sum
WACC	Weighted Average Cost of Capital
WT	Wind Turbine
XLPE	Cross-linked polyethylene

1 Preface

1.1 Project's Origin

This project comes as the continuation of the Research Assignment performed by Cristoph Kaufmann. From CITCEA-UPC, a technology transfer center from Technical University of Catalonia (UPC BarcelonaTech), the need of studying the collection grid of an offshore wind farm was presented in view of reducing the investment required.

1.2 Motivations

Renewable energy has suffered an exponential grown in the last decades, this is a consequence of a higher social awareness about the climate change, outcome of the traditional ways to generate energy and industrial development.

Climate change is one of the greatest challenges facing mankind because environmental well-being and economic growth are heavily inter-linked. Nowadays, the effects of the climate change have already shown up as the global warming, the rising sea level or the increase of extreme storms or droughts. Therefore, there is an urgency to reduce the causes of it, and mainly the emissions of greenhouse effect gases.

Hence the motivation to work upon wind power as it is positioned as one of the most common alternative to get clean energy nowadays, along with solar and tidal power thanks to the technological breakthrough in equipment and methods and a better understanding of the wind, solar and sea resources.

2 Introduction

Wind energy has experienced tremendous advances in the last decade. In addition, the situation looks like it will continue to proliferate. According to International Energy Agency (IEA) the wind-generated production in 2035 will be 2182 TW that nearly doubles the production in 2020 that is forecast to be 1282 TW [1]. Offshore wind capacity is expected to almost triple to nearly 52 GW in 2023, dividing the growth between the European Union and China and other Asian countries [2].

As the prime quality wind locations have been used, an attractive alternative for the location of wind farms is to build offshore, as also the installation restrictions offshore are considerably lower which allows the usage of larger wind farms. The design process of an offshore wind power plant needs to take into account the environmental conditions expected at a site over the offshore wind project's lifetime. These environmental conditions primarily refer to the wind, wave, water depth and soil and seabed characteristics. Parameters as the wind speed, the wind direction or the turbulence intensity, are crucial in finding the optimal layout in order to maximize the energy generation [3].

Productivity may be greater at the sea than on land because there is less friction between wind and water and the wind flow pattern is more uniform, therefore as being more steadier the source of energy is much more reliable.

The wind speed in offshore locations tends to be faster than in onshore ones. Small raises in wind speed elicits a large increase in energy generation: a turbine in a 24 km/h wind speed can generate twice as much energy as a turbine in a 19 km/h wind speed. So the same wind farm offshore can generate much more power than onshore [4].

A given site will have a frequency distribution of wind direction, e.g. a coastal region may have winds that primarily come from the sea whereas in a flat region the winds may come from the direction of nearby mountains. When sufficient wind measurements are made at a site, it is common to create a wind rose, as a repository of all the wind data, which gives the relative frequency of wind coming from each direction. An example of a wind rose can be found in Figure 1 where the radius of the widest wedge shows the time that the wind blows from a particular direction; the radius of the second wedge shows the sector contribution to average wind speed; the solid (red) wedge gives the energy content of the wind in that direction.

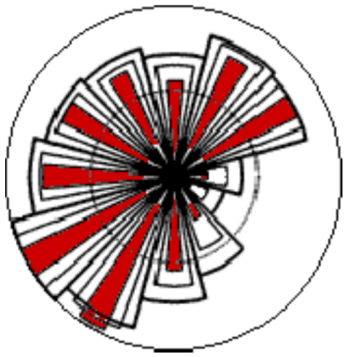

Figure 1: Wind rose for Brest, France [5].

The levels of environmental turbulence offshore are lower in comparison at onshore locations. Standard turbulence values at turbine hub height are 6-8% offshore meanwhile 10-12% over land. Even though this may not turn out as a decrease in loads on offshore wind turbines on account of the high levels of wake-generated turbulence in wide wind farms [6].

Offshore wind power is cheaper than solar photo-voltaic, gas, coal and nuclear, actually is the 2nd cheapest manner to generate power in Europe, behind onshore wind power. And due to more powerful and bigger turbines, it is said that the costs of offshore wind power will continue to diminish [7].

The mainly environmental issues concerning offshore wind power plants are the effects on the fauna and flora, pollution from increased vessel traffic or release of contaminants from seabed sediments. On the other hand, a new habitat is introduced by the wind turbine foundations as they act as pseudo-reefs so the shellfish is attracted thus the animals that feed on them are as well [8, 9]. However these effects are still under study. In addition, the visual impact, elevated noise levels and the appearance of an electromagnetic field may difficult the operation of maritime radio systems, civil, military and aeronautical radars as well as navigational aid systems.

2.1 Objectives of the Project

There are two different types of cables in an Offshore Wind Power Plant (OWPP), export cables and array cables , also known as inter-array cables. Both are used for the passage or transmission of generated electricity by the wind turbines. The former connect the offshore substation with the grid or substation on land; these cables are excluded from this study. And the last ones carry the generated power from several wind turbines to the collector system located in the offshore substation.

In order to choose the right cables needed there are some factors that need to be taken into account such as the power losses of the cable or the investment required for the wiring.

Therefore, the main aim of this thesis is to optimize the cable sizing of 3 different scales of OWPP relying on reducing the power losses and total costs. It is based on the Research Assignment of Cristoph Kaufmann [10], who achieved his goal by the usage of a multi-objective function and finding the optimal point of the Pareto-front.

2.2 Scope of the Project

This project has the intention of optimizing the cables sizes of a wind farm regarding the election of the array cables in order to reduce costs and power losses. The optimization is performed through multi-objective function and Pareto efficiency. The number of cross-sections of the cable available is limited to three in the case of the optimization. The power flow is calculated to precisely model the cable losses at full load, this procedure is contrasted with cable sizing method based on thermal rating, which is used as the reference design of the wind farm. The calculus and operations are programmed and solved with the software MathWork's MATLAB.

Towards to accomplish the objectives of this thesis, there are certain subjects of knowledge to be considered:

- Structure and cables in an offshore wind power plant (OWPP).
- Electrical design, focused on the cables.
- Newton-Raphson Method and Pareto Front Theory.
- Cost models.
- Matlab software.

A fundamental step on this thesis is the understanding of Cristoph Kaufmann's Research Assignment, which includes all the code used to optimize the cable sizing of a wind farm composed by 49 wind turbines as the desire is to obtain the optimization of a wind farm formed by 49, 70 and 100 Wind Turbines (WT) with the difference of the rated voltage.

The following chapter is an overview of the previous knowledge required above-mentioned. Afterward, with acquaintance of the topic, the methodology followed is explained as well as the baseline wind farm from Cristoph Kaufmann's Research Assignment and two methods for enlarging the wind farm. Here under, the case study for this thesis is presented likewise the results obtained by applying the principles and theory explained in the previous chapters. Finally, conclusions are drawn and a standpoint is given.

3 Fundamentals

The aim of this chapter is to provide an overview about offshore wind power plants, focusing on its collection grid area; electrical design of the collector system with the purpose of calculating the power losses, a brief summary of the Newton-Raphson method and the Pareto Front theory and the cost models in order to evaluate the costs of the design.

3.1 Offshore Wind Power Plants

Offshore wind technology provides new locations with higher wind resources, as it is steadier. Since offshore wind farms can be build in short time and close to populated coastal areas, they have a major part in the decarbonization of the energy sector. The combination of large-scale sites, lower installations restrictions and higher capacity factors make offshore wind an appealing choice for utility-scale low-carbon electricity.

Most of the capacity installed and operating for offshore wind to date is located off northern Europe [11], with Europe being the continent with a major number of wind farms followed by Asia as can be seen in Figure 2.

Figure 2: Map with an overview of the number of wind farms and capacities by continents.

The Figure 3 displays the layout of Horn Rev, an offshore wind farm placed in the North Sea (in Denmark). The dashed line closes the area known as collection grid, formed by the wind turbines each interconnected by buried cable network, in radial topology, and the offshore substation platform. The wind turbines form an oblique matrix with 8 rows and 10 columns, spaced with 7 rotors diameters in both directions. The generated power, collected by the offshore substation, is transmitted to the onshore grid by an HVAC-link, known as external cable.

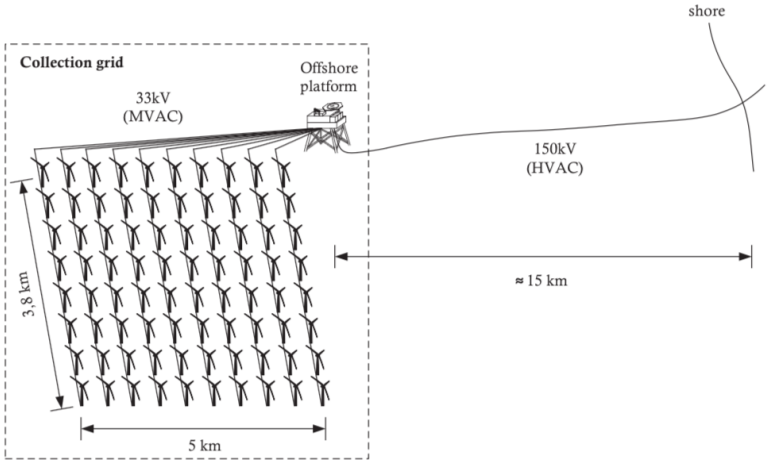

Figure 3: Horns Rev offshore wind farm layout [3].

The design process of an OWPP demands exhaustive studies since it involves many features besides the prevailing wind speed and direction such as maintenance and operational tasks. The turbine spacing and the orientation of the turbine rows are important considerations that need to be taken into account in order to minimize the so called array losses, which is a reduction in the available wind, at the wind turbine, by neighbouring wind turbine rotors. In Europe, turbines are spaced between 5-9 rotor diameters apart in the incoming wind direction and between 3-5 diameters apart in the direction perpendicular to the incoming winds.There are different possible connections designs known as radial, star and ring which are shown in the figures below.

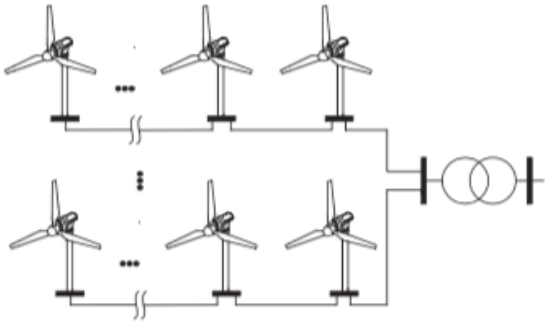

Figure 4: Radial collection configuration.

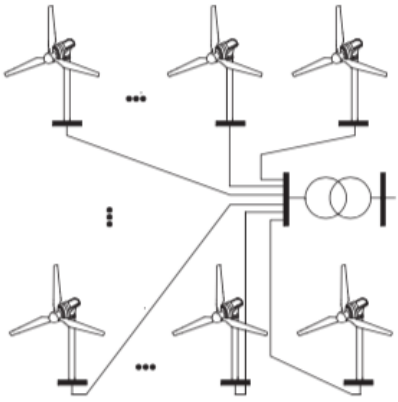

Figure 5: Star collection configuration.

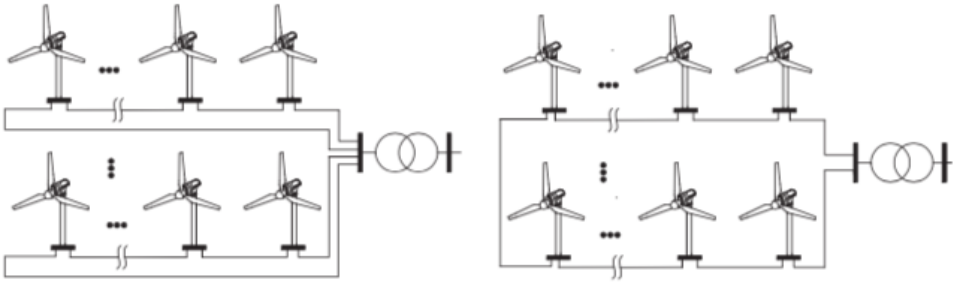

Figure 6: Ring collection configuration.

The most usual, cheap and simple is the radial collection configuration presented in Figure 4, the feeder connects the WT with the substation in string configuration. The maximum number of wind turbines that can be connected to one feeder is limited by the cable ampacity and the rated power output of the generators. Even though it is not as reliable since in case of failure in one cable section or a failure of the switch-gear at the hub end, all the power generated by the downstream wind turbines in the string will be lost [3, 12, 13].

Following, a brief description of the components of an offshore wind farm is presented.

3.1.1 Offshore Substations

The main role of the substation is to collect the power generated by the wind turbines and transform it from Medium Voltage Alternating Current (MVAC) to High Voltage Alternating Current (HVAC) in order to transfer the electricity to the grid onshore and reduce the electrical losses in this transmission.

It houses electrical components including transformers, switch-gear an control systems, as well as other equipment such as cranes, back-up power systems, safety equipment, among others.

The offshore substation is the most complex single component of the wind farm [14].

3.1.2 Wind Turbines

Modern wind turbines are three-bladed, which has shown to be the optimum number of blades in electrical energy production. In an OWPP the blades of the wind turbine tend to be bigger than onshore, since the area of the wind farm can be larger.

The most common WT can be classified into four types depending on their ability to control speed:

- Fixed speed wind turbine.
- Partial variable speed wind turbine.
- Variable speed wind turbine with partial rate converter.
- Variable speed wind turbine with full rate converter.

Today's wind turbines are of the variable speed design, incorporating the pitch control and power electronics The two variable-speed configurations available are the partial rated converter also known as the Doubly Fed Induction Generator (DFIG) wind turbine and the Fully Rated Converter (FRC) wind turbine. The DFIG, shown in Figure 7, wind turbines use induction machines with high controllability, running at super or sub-synchronous speed; a low-speed shaft and a high-speed shaft linked by a gear-box; and a half-rated power converter. Meanwhile the FRC, shown in Figure 8, wind turbines use multi-pole synchronous generators of short axial length and long radial length. One low-speed shaft for direct connection with the wind prime-mover (i.e. no gear box is used).

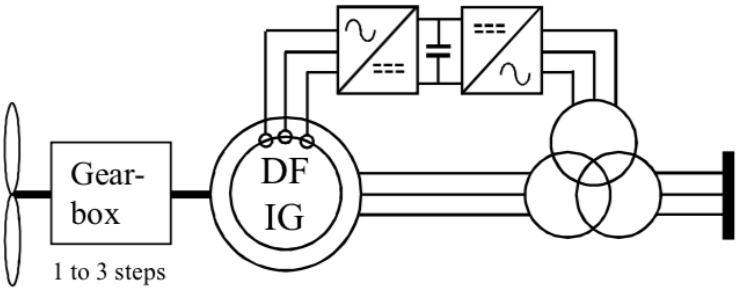

Figure 7: Variable speed wind turbine with DFIG [15].

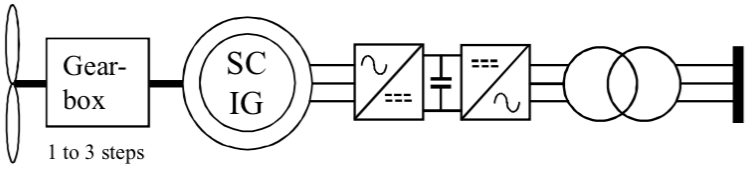

(a)

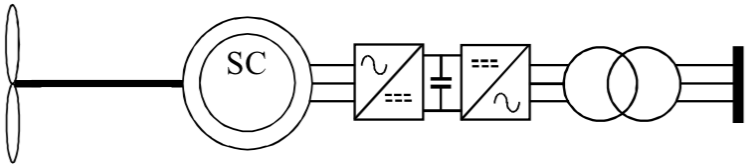

(b)

Figure 8: (a) Variable speed wind turbine with full rate converter SCIG and (b) direct drive SC [15].

3.1.3 Cables

As well said in Section 2.1, there are two different types of cables in an OWPP, export cables and array cables. This thesis only focuses on the latter.

Towards the transmission of power, AC cables can be differentiated into two types, single-core or three-core cables (Figure 9). The former one relates when the three phases are separated by a certain distance from each other, they are usually called 3x1-Core cables. The latter is 1x3-Core cable where the three phases are in insulated cores bundled together in trefoil configuration, made of copper (normally) or aluminum (for cost and weight reduction but for small power ratings), all surrounded by a common shield and armouring. Three-core cables have more benefits than drawbacks compared to the single-core cables regarding offshore wind farms, therefore are more used. The power losses are lower due to the cancellation of the magnetic field between the three cores. In addition, is possible to integrate communications into the three-core configuration, thus no extra fiber optic cable needs to be laid, saving cost. Furthermore, the cable is laid in one instance and ergo the installation is significantly cheaper than single-core cables. However, the handling and the installation is more laborious than single-core cables owing to the heavier weight, entailing a restriction in the depth of the laying cable [16]. Besides, making cable joints are slightly more problematic for three-core cables and in case of a single failure in one of the three cores the damaged cable needs to be replaced with a whole new cable instead of only replacing the single phase cable affected in the case of single-core cables [17].

(a) (b)

Figure 9: (a) Single–core cable with lead sheath and wire armour.
(b) Three–core cable with optic fibers, lead sheath and wire armour [18].

XLPE is the recognized abbreviation for cross-linked polyethylene. XLPE and other cross-linked synthetic materials, like EPR, are being increasingly used as cable insulants for a wide range of voltages in submarine cables [19]. The effect of cross-linking is to block the movement of molecules regarding each other under the stimulation of heat which gives stability at elevated temperatures (near 100 degrees), this permits operating at higher temperatures so that an XLPE cable has a high current rating and resist high electrical stresses. With XLPE insulation, the dielectric losses can be neglected in comparison to the conductor losses and resulting from its increased toughness, the thickness of the insulation can be slightly reduced compared to PVC [20]. In addition, other sheets of lead sheath or aluminum are applied over each core for water isolation in case of using XLPE. This additional isolation is not needed in case of using EPR though [21, 22]. Additional layers based on polypropylene can be applied for corrosion protection as well as a galvanized steel wire armour in order to increase the tensile strength for submarine applications [3, 23].

So, XLPE cables consist of the following components [24]:

- Conductor: Copper (Cu) or Aluminum (Al) stranded compacted conductor; Cu segmental conductor; Cu or Al conductor with key-stone shaped profiles; Longitudinal eater sealing of conductor.
- Triple extruded and dry cured XLPE insulation system.
- Metallic screen: Copper wire screen; Copper tape screen; Radial water sealing, Al or Cu laminate solidly bonded to outer polyethylene jacket or lead sheath; Longitudinal water sealing of metallic screen.
- Non-metallic outer sheath: PVC; Halogen free flame retardant; Co-extruded conductive layer over the sheath for special sheath testing.
- Armour: Single wire armour; Double wire armour.

3.2 Electrical Design

Several decisions must be made before starting to build the model that will describe the wind farm with the aim of finding the optimal electrical layout [25]. The extend of the electrical design of the collector system in this thesis involves the cables solely. Hence, the boundaries of the analyzed system are the substation and the grid-sourced converter of each wind turbine, respectively. Similarly to other topic-related studies like [26, 27, 28], a π-model is adopted to depict each section of cable between two nodes of the collector system as a lumped circuit. By applying this scheme, the power losses in steady-state conditions are calculated.

Subsequently, the basal equations of the π-model are described, followed by the explanation of the power flow analysis.

3.2.1 Cable Model

There are several mathematical models to describe a transmission line depending on the analysis and the desired outcomes of the power system. A power cable can be modeled as a transmission line taking into account its own specific electrical characteristics. An overhead transmission line which is less than 240 km long can be modeled by a lumped element π-model as shown in Figure 10, [29], the lumped π-model is also applicable for an underground or submarine cable with less than 100 km of length [30]. Longer transmission lines have to be modeled by means of the distributed element model, in which the line parameters are distributed continuously throughout the line and can be regarded as infinitesimal small elements [27, 29]. Other models, involving partial differential equations are computationally costly and give extra information which is not needed. Instead, an algebraic model of a line as a lumped-circuit opens up the status at both ends of a line with cheaper computational cost.

The core of the π-model, which calculates the cable power losses, is based on a method derived by Anders and Brakelmann in [31]. Since the time-varying actions are small, the use of an algebraic description and the hypothesis of steady-sate operation of a power system is justified.

Figure 10 represents the π-model of a cable section, it is described by the following parameters as in [32]:

- Series parameters:
  - R_s: series resistance per kilometer of cable and per phase, measured in $\Omega{\cdot}km^{-1}$.
  - X_s: series reactance per kilometer of cable and per phase, measured in $\Omega{\cdot}km^{-1}$.
- Shunt parameters:
  - B_p: shunt susceptance per kilometer of cable and per phase, measured in $S{\cdot}km^{-1}$.
  - G_p: shunt conductance per kilometer of cable and per phase, measured in $S{\cdot}km^{-1}$.

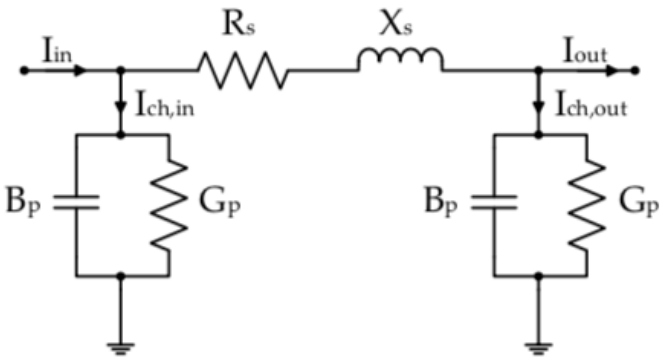

Figure 10: Lumped element π-model of a power cable.

The series impedance (due to line resistance and inductance) as well as the shunt admittance (due to shunt capacitance and conductance) are summed up to single electrical components, so these parameters depend on the conductor and geometric arrangement and hence, are specific for the cable configuration. In the case of the π-model depicted in Figure 10, in symmetric steady-state conditions at both ends, the model parameters are defined as

$$\underline{Z} = R_s + jX_s \tag{3.1}$$

$$\underline{Y} = G_p + jB_p \tag{3.2}$$

It is important to pay special attention to the equation 3.2, where the admittance is calculated, because in this example the both shunt elements $\underline{Y}$ are assumed to be identical for both nodes, which enacts the case of homogeneous lines of equal lengths (i.e. symmetric lines) but they could be different in other cases representing asymmetric lines.

Cable Resistance

The resistance of the conductor is a design parameter to take into account, as it enables the estimation of the current carrying-capacity, also known as ampacity, and the resulting operating temperature [33, 34].

Depending on the type of current supplied, the current density throughout the cross-section can be either uniform in the case of supplying Direct Current (DC) in homogeneous conductors, or not uniform when supplying Alternative Current (AC), due to the skin and proximity effects [33, 35, 36].

The skin effect is known as the preference of an alternative current to concentrate the current density near the surface of the conductor on a level called the skin depth, which is inversely proportional to the frequency as can be seen in Figure 11, where the first cross-section starting from the left is conducting DC current, the middle one is conducting low-frequency AC current and the last one is conducting high-frequency AC current [37]. The ohmic resistance of the conductor is increased due to the concentration of current on the surface of the conductor [38], and leads to a temperature rise limiting the conductor's ampacity. At high frequencies the current tends to be concentrated towards the periphery of the conductor [39], hence increasing the AC resistance and power loss in the conductor [40].

Figure 11: Representation of skin depth (painted in red) depending on the conducting current.

The proximity effect is known as the situation when two or more conductors are close to each other so that the alternating magnetic field of each one, caused by the AC flow through a conductor, induces eddy currents in the adjacent conductors altering the distribution of the current along the conductor. Due to this interaction, the current is concentrated in areas of the conductor farthest away from nearby conductors when carrying current in the same direction (Figure 12a), since the magnetic fields of the halves of the the conductors which are close are cancelling each other therefore no current flow through that halves portion of the conductor. If the conductor carries the currents in opposite directions (Figure 12b), the magnetic field of the far off half of the conductor cancel each other so the current is zero in the farthest half of the conductor.

(a) (b)

Figure 12: Representation of current density if the current flows (a) in the same direction, (b) in the opposite direction.

In this thesis, the analytical model adopted to approximate the resistance of the cable is explained in [33]. As it refers to the internationally recognized IEC 60287-1-1 standard [41] the outcomes are assumed to be enough accurate for the frequency 50Hz. The total AC resistance R_{AC} for XLPE cable is calculated by the following equation extracted from the IEC 60287-1-1 standard:

$$R_{AC} = R_{DC}(1 + y_s + y_p) \qquad [\Omega m^{-1}] \tag{3.3}$$

The R_{AC}/R_{DC} resistance ratio can be an indicator of the fluctuation in the AC resistance of a conductor. The equation 3.3 calculates the R_{AC} by the resistance from the direct current resistance (R_{DC}) and the addition of some other factors which will be characterized here-under.

Firstly, the DC resistance of the conductor has to be computed taking into account the first effect, which is the change of the DC resistance at different operating temperature θ under load conditions:

$$R_{DC,\theta} = \frac{\rho_{20}}{S}[1 + \alpha_{20}(\theta - \theta_0)] \tag{3.4}$$

It is calculated by interpolating the material dependant resistivity (ρ_{20}) at θ_0 = 20^{o}C over the conductor's cross-section S. Where α_{20} is the temperature coefficient at 20^{o}C and θ the operating temperature.

Following, the skin effect becomes especially important for large conductors sections or at high supply frequencies, where the skin depth δ is smaller. The skin depth in a conductor is calculated as

$$\delta = (\pi f \mu_r \mu_0 \sigma)^{-1/2} \tag{3.5}$$

where f is the supplied frequency, μ_r the relative permeability of the material of the conductor, μ_0 the permeability of the air or free space and the σ is the electrical conductivity. It can be seen that the skin depth decreases for increasing values of f, μ_r and σ.

The skin effect is reflected in equation 3.3 by the y_s factor, which can be calculated, according to [41], as

$$y_s = \frac{x_s^4}{192 + 0.84x_s^4} \tag{3.6}$$

where

$$x_s^4 = \left(\frac{8\pi f K_s}{R_{DC} 10^7}\right)^2 \tag{3.7}$$

In the case of solid round conductors, the constant K_s = 1. If the conductor is isolated from the rest, then the R_{AC} can be calculated by

$$R_{AC} = R_{DC}(1 + y_s) \qquad [\Omega m^{-1}] \tag{3.8}$$

However, to obtain accurate results (3.8) is only applicable when $x_s \leq 2.8$ if not the formula is not accurate to approximate the skin effect.

Finally, the proximity effect of three parallel conductors carrying three-phase currents is considered because of the three-core XLPE conductors mentioned in Section 3.1.3. The IEC 60287-1-1 standard propose the following approximation to calculate the proximity factor y_p as

$$y_p = \frac{x_p^4}{192 + 0.84x_p^4}(d_c/s)^2 \left[0.312(d_c/s)^2 + \frac{1.18}{\frac{x_p^4}{192+0.84x_p^4} + 0.27} \right] \tag{3.9}$$

where

$$x_p^4 = \left(\frac{8\pi f K_p}{R_{DC} 10^7} \right)^2 \tag{3.10}$$

In the case of copper round solid conductors, the constant $K_p = 1$. The diameter of the conductor is characterized by d_c and the distance between conductors' axes by s, when the three conductors are equally spaced and $s = (s_1 \cdot s_2)^{1/2}$ when the spacing between adjacent phases is not equal, according to [41].

So, with all these factors the AC resistance can be calculated by equation 3.3.

Cable Inductance and Shunt Capacitance

The inductance per meter [H/m] of either flat or trefoil formation of three-core cables can be calculated by the equation 3.11 [42] or either it can be given by the manufacturer. With $N = 1$ corresponds to a trefoil formation and with $N = 1.26$ to a flat formation, shown in Figure 13, d_c corresponds to the diameter of the conductor in mm and s represents the distance between the conductor axes in mm. Some typical values of the constant K for different conductors can be found in Table 1.

$$L = \left(K + 0.2ln\left(\frac{2Ns}{d_c} \right) \right) 10^{-6} \tag{3.11}$$

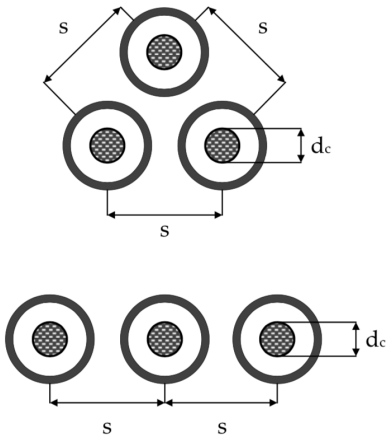

Figure 13: Trefoil and Flat formation of three single-core cables.

Typical values for constant K	
Number of wires in conductor	K
3	0.0778
7	0.0642
19	0.0554
37	0.0528
61 and over	0.0514
1 (solid)	0.0500
Hollow-core conductor, 12mm duct	0.0383

Table 1: Typical values for constant K for different stranded conductors at 50Hz [42].

The inductive reactance X_s of the impedance computed in equation 3.1 of a cable section can be calculated by

$$X_s = 2\pi f L \tag{3.12}$$

where f is the frequency in the collector system of 50 Hz and L is the inductance either given by the manufacturer or calculated by the equation (3.11).

The shunt conductance of the submarine cable is very small, and thus neglected ($G_p \approx 0$) according to [43]. Therefore, the shunt admittance is only affected by the shunt susceptance (B_p see equation 3.2), which is only affected by the capacitance of the capacitor and the frequency as can be shown in the following equation:

$$X_c = -\frac{1}{2\pi f C} \tag{3.13}$$

where

$$C = \frac{\varepsilon}{18 ln\left(\frac{D_i}{d_c}\right)} 10^{-9} \tag{3.14}$$

in which ε represents the relative permittivity of the insulation material, D_i is the external diameter of the insulation in mm (excluding the screen) and d_c is the diameter of the conductor in mm (including the screen, if any). As well as the inductance, the capacitance can either be given by the manufacturer or calculated by the equation (3.14).

So, the shunt admittance is calculated by

$$\frac{\underline{Y}}{2} = j\pi f C \tag{3.15}$$

Lastly, in order to incorporate all cable parameter into the π-model described formerly, each parameter needs to be multiplied by the euclidean length $l_{i,j}$ of the vector between the WT i and j to obtain the quantity of the entire cable section, the parameters that need this adjustment are inductive reactance of the impedance (X_s, equation 3.12) and the shunt admittance ($\underline{Y}$, equation 3.15) since are given by kilometer length.

Cable Sizing

In manifold studies like [44, 45] the method for cable sizing an OWPP is the conventional one, based on the usage of the current carrying capacity of a cable at steady-state conditions as a way for determining the cable size. Working in this conditions can assure that the conductor temperature will not exceed its operational limit if that particular current is applied continuously. This upper limit reduces the rate of thermal aging of the insulation [44].

It is said by Walling and Rudy in [45] that applying only the thermal rating will not result in an economically optimal collector system design. Therefore, Catmull in [44], offers a method to derive cyclic load profiles of the cables resulting in a reduction of the cable sizes meaning as well project costs.

The thermal method for cable sizing is used as a reference design, representing the conventional design method.

3.2.2 Power Flow Analysis

Once the π-model is specified with all the equations, the collector system can be modelled by means of the equivalent π-model for each cable section of the structure of the wind farm. Obtaining the power losses in steady-state by solving the system of complex variables is a major problem of power flow analysis. Each node in the system is connected to various nodes either injecting or removing power from the collector system, which is akin to a transmission system but with load and generator buses [46].

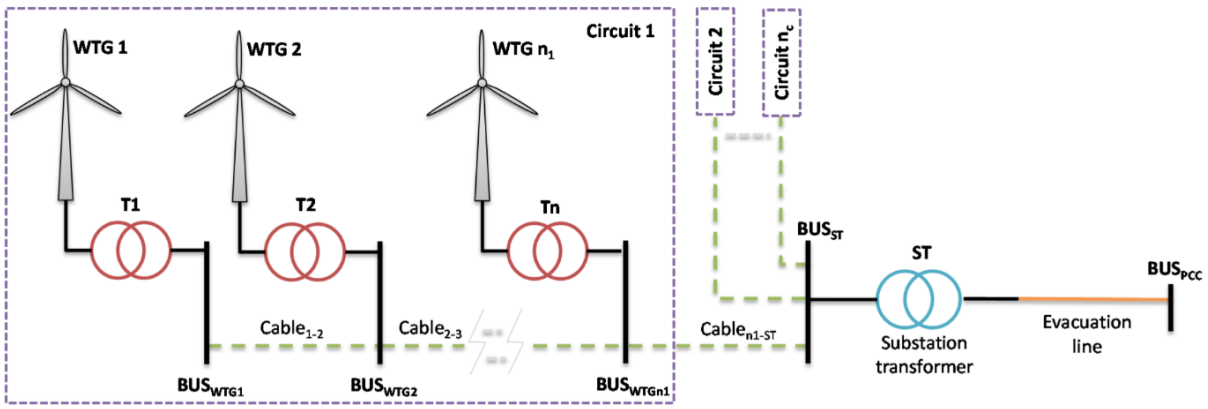

Figure 14: Single-line diagram of a wind farm [47].

A graphic example of one feeder of the collector system as a single-line diagram is shown in Figure 14. Each wind turbine *WTG* stands for a bus in the system BUS_{WTG_n} and are connected by the cable named $Cable_{1-2}$ for the first and second wind turbine of the feeder, while the cable connecting the last wind turbine and the substation is named $Cable_{n1-ST}$. In this way, cables with higher ampacity are required since the generated power of each wind turbine is injected in the cable, so the current transported through the cable increases. Therefore, the π-model described is not symmetric. In order to force the current flow from the wind turbines to the substation, the voltage at each wind turbine must be higher than the voltage at the substation. The feeders are illustrated as numbered circuits n_c in the radial configuration of the collector system presented in Section 3.1. All feeders are connected to the substation by the BUS_{ST} and from there with the common coupling point BUS_{PCC} through the substation transformer and exporting transmission lines.

Power flow problems can be described by four variables for each bus (node *i*) according to [32]:

- V_i : voltage magnitude.
- θ_i : voltage angle.
- P_i : net active power (algebraic sum of generation and load).
- Q_i : net reactive power (algebraic sum of generation and load).

Depending on the known and unknown variables, three bus types can be defined in power flow calculations according to [32]:

- PQ bus : P_i and Q_i are known, whereas V_i and θ_i are unknown.
- PV bus : P_i and V_i are known, whereas Q_i and θ_i are unknown.
- Vθ : V_i and θ_i are known, whereas P_i and Q_i are unknown.

PQ buses are habitually used to represent load buses without voltage control, also are the most common bus type of all buses. PV buses are used to represent generation buses with voltage control. Lastly, the Vθ bus, also called slack bus or reference bus, is used in two situations in power flow calculations. Firstly, it gives the voltage angle reference (θ_0) for the power system. Secondly, because the active power losses are unknown before the calculation so Vθ balances generation, load and losses by generating active power [32, 46].

The balance of generation (P_{Gi} and Q_{Gi}) and demand (P_{Di} and Q_{Di}) is a representation of the active and reactive power of each node or bus *i* in the collection system, a positive sign means that the power injected is greater than the power absorbed, while a negative sign indicates a higher demand of power. For the bus *i* it can be expressed in the general form as

$$\underline{S_i} = P_i + jQ_i = (P_{Gi} - P_{Di}) + j(Q_{Gi} - Q_{Di}) \tag{3.16}$$

The use of Kirchhoff's circuit laws to calculate all currents I in terms of voltage V would lead to a very large system of linear equations for realistic power systems become very large [46]. Hence, the matrix notation is used in the following.

Is assumed that the collector system in steady-state conditions is balanced in the three-phase system. From the nodal analysis of the system, for each bus, the injected current can be calculated as

$$\underline{I} = \underline{Y_{bus}}\underline{V} \tag{3.17}$$

where $\underline{I}$ and $\underline{V}$ are nodal current and nodal voltage respectively, in form of n-vectors and $\underline{Y_{bus}}$ is the n x n nodal admittance matrix. The symmetric nodal (or bus) admittance matrix $\underline{Y_{bus}}$ includes all circuit elements, where the diagonal elements are the self-admittance $\underline{y_{ii}}$ of bus i and the rest of elements $\underline{y_{ik}}$ represent the element connecting the nodes i and k. It is important to note that $\underline{y_{ik}}$ is non-zero only where a physical connection exists between the two nodes [46]. These precepts can be defined as

$$\underline{y_{ii}} = \sum_{i=1}^{n} \text{all admittances of } \pi\text{-equivalent circuit elements that connect bus } i \tag{3.18}$$

$$\underline{y_{ij}} = -\text{admittance of } \pi\text{-equivalent circuit element bridging the } i\text{th and the } k\text{th buses} \tag{3.19}$$

Since many zero entries are present in the resulting bus admittance of realistic power systems, equation 3.2 is recalled to obtain the element $\underline{y_{ik}}$ of the admittance matrix $\underline{Y_{bus}}$ by

$$\underline{y_{ik}} \triangleq g_{ik} + jb_{ik} \tag{3.20}$$

for each π-equivalent circuit element. The bus current of node i, using equation 3.17 will be given by

$$\underline{I_i} = \sum_{k=1}^{n} \underline{y_{ik}}\underline{V_k} \qquad i = 1, 2, 3, ..., n \tag{3.21}$$

With this definition of the current, according to equation 3.16 the apparent complex power of node i can be calculated by [46]

$$\underline{S_i} = \underline{V_i}\underline{I_i^*} = \underline{V_i}\left(\sum_{k=1}^{n} \underline{y_{ik}}\underline{V_k}\right) \qquad i = 1, 2, 3, ..., n \tag{3.22}$$

This equation is named fundamental power flow equation. Special attention needs to be paid to the fact that the complex voltage use a polar form while the complex admittance use a rectangular form. Therefore, the complex voltage can be represented as [46]

$$\underline{V_i} \triangleq |\underline{V_i}|e^{j\angle V_i} = |V_i|e^{j\theta_i} \tag{3.23}$$

$$\theta_{ik} \triangleq \theta_i - \theta_k \tag{3.24}$$

Hence, with equation 3.20 an equivalent form of the fundamental power flow equation (3.22) can be written as [48]

$$\underline{S_i} = \sum_{k=1}^{n} |\underline{V_i}||\underline{V_j}|e^{j\theta_{ik}}(g_{ik} - jb_{ik}) \tag{3.25}$$

$$\underline{S_i} = \sum_{k=1}^{n} |\underline{V_i}||\underline{V_j}|(\cos\theta_{ik} + j\sin\theta_{ik})(g_{ik} - jb_{ik}) \qquad i = 1, 2, 3, ..., n \tag{3.26}$$

Taking the real and imaginary parts of equation 3.26:

$$P_i = \sum_{k=1}^{n} |\underline{V_i}||\underline{V_j}|(g_{ik}\cos(\theta_i - \theta_k) + b_{ik}\sin(\theta_i - \theta_k)) \qquad i = 1, 2, 3, ..., n \tag{3.27}$$

$$Q_i = \sum_{k=1}^{n} |\underline{V_i}||\underline{V_j}|(g_{ik}\sin(\theta_i - \theta_k) - b_{ik}\cos(\theta_i - \theta_k)) \qquad i = 1, 2, 3, ..., n \tag{3.28}$$

$$\text{where,} \quad \theta \triangleq \angle\underline{V_i}$$

By this, all fundamental equations of the power flow system are defined. Remark that the slack bus Vθ acts as a reference and balance for the power system, and it is presumed to be the first bus in the system. That is why the first bus is known and has no equation [32].

Hereafter, a method to express the system quantities as fractions of a defined base unit quantity is presented.

3.2.3 Per-unit System

In power system analysis sometimes large numbers of transformers may be encountered or variation of voltage may occur in the circuit, therefore the per-unit system is used. It is defined as the ratio of actual value in any unit and the base or reference value in the same unit. Any quantity is converted into per-unit quantity by dividing the numeral value by the chosen base value of the same dimension [49]. The per-unit value is dimensionless. It simplifies the calculations as the values are taken in the same unit.

The per-unit system can be formulated as

$$\text{Per-unit value} = \frac{\text{true value}}{\text{base value of the quantity}} \tag{3.29}$$

The base values can be chosen arbitrarily, the most common are [49]:

- Base voltage : rated voltage of the machine.
- Base current : rated current of the machine.
- Base impedance : base voltage /base current.
- Base power : base voltage · base current.

The base voltage V_{base}, defined as line-to-line voltage, and the base power S_{base} can be selected in a convenient way for the analysis. Their choice automatically sets the other base values. The base current per phase I_{base} for a three-phase system can be calculated by

$$I_{base} = \frac{S_{base}}{\sqrt{3}V_{base}} \tag{3.30}$$

and the base impedance Z_{base} by,

$$Z_{base} = \frac{V_{base}^2}{S_{base}} \tag{3.31}$$

With this method, the percentage of voltage drop can be directly read off by the per-unit voltage. Generally, different values in the system can be compared easily.

3.3 Newton-Raphson Method

Since large systems of power flow problems cannot be solved analytically, an iterative strategy can be programmed and employed to compute the solution. There are two generally-known solution methods. The first method is the Gauss iteration, which has a more developed variant called Gauss-Seidel method. The second one is the Newton-Raphson method, which allows fewer iterations and faster convergence than the Gauss and Gauss-Seidel method. In addition, the results obtained are more precise. Even though, all this advantages require larger memory [32, 46]. Hence, the method chosen as an iterative strategy for this thesis is the Newton-Raphson method.

The Newton-Raphson method is an effective method for solving non-linear algebraic systems numerically. It is based on the simple idea of linear approximation [50] and it can be written as

$$f(x) = 0 \tag{3.32}$$

where f is an n-vector function of x, which is a n-vector of unknowns. Letting $f(x)$ be a well-behaved function and r be a root of the equation 3.32, the process starts with an estimate x_0 of r. From x_0, an improved estimate x_1 is obtained. From x_1, a new estimate x_2 is produced. This process is ongoing until the estimate x_v is close enough to r or until it becomes clear that there is no solution. This general style of proceeding is called iterative [50].

In order to find the roots of the system, the starting value x_0 needs to be chosen carefully since the Newton-Raphson works nearly perfectly if x_0 is close to r but it can work terrible if it is not. The vector equation is solved by the next sequence [32]:

$$J(x_v)\Delta x_v = -f(x_v) \tag{3.33}$$

with,

$$x_{v+1} = x_v + \Delta x_v \tag{3.34}$$

where v represents the iteration number, Δx_v the correction vector and $J(x_v)$ the Jacobian matrix. With the purpose of obtaining $f(x)$ at x_v, Taylor series expansion is used to linearise the function and thus ensues

$$f(x_v + \Delta x_v) \approx f(x_v) + J(x_v)\Delta x_v \tag{3.35}$$

Once the equation is linearized, the correction vector Δx_v can be calculated applying the Gaussian elimination of

$$f(x_v) + J(x_v)\Delta x_v = 0 \tag{3.36}$$

Andersson [32] realized a compact structure of the Newton-Raphson algorithm for the n-dimensional case as follows:

1. Set v = 0 and determine a correct starting value x_0
2. Compute $f(x_v)$
3. Test the convergence: If $|f_i(x_v)| \leqslant \varepsilon$ for i = 1,2,3, ... ,n , then x_v is the solution. If not, go to step 4
4. Compute the Jacobian matrix $J(x_v)$
5. Update the solution to
$$\Delta x_v = -J(x_v)f(x_v) \tag{3.37}$$
with,
$$x_{v+1} = x_v + \Delta x_v \tag{3.38}$$
6. Update iteration counter to v+1 and go to step 2.

Knowing the essential working principle of the Newton-Raphson method, it can be applied to the power flow equations.

Application of the Newton-Raphson Method to the resolution of the Power Flow Equations

Since depending on the bus type (see pg. 19) certain variables are unknown, voltage magnitude and voltage angle in a PQ bus or reactive power and voltage angle in PV bus, the aim is finding these unknown properties applying the Newton-Raphson method to the power flow equations 3.27 and 3.28.

The state vector x is composed by [46]

$$x = \begin{bmatrix} \theta \\ |V| \end{bmatrix} \tag{3.39}$$

in which θ represents the unknown voltage angles and $|V|$ the voltage magnitudes. Likewise, the first components of the non-linear function f represent the active power and the last ones the reactive power, with a structure as [46]

$$f(x) = \begin{bmatrix} \Delta P(x) \\ \Delta Q(x) \end{bmatrix} \tag{3.40}$$

with,

$$f(x) = \begin{bmatrix} P_2(x) - P_2 \\ \vdots \\ P_m(x) - P_m \\ Q_2(x) - Q_2 \\ \vdots \\ Q_m(x) - Q_m \end{bmatrix} \tag{3.41}$$

where the functions $P_i(x)$ and $Q_i(x)$ are the active and reactive power flows of node (bus) i calculated with equations 3.27 and 3.28, respectively. And P_i and Q_i are the already known active and reactive power injection at from generators and loads at node (bus) i. It is important to remember that the first bus is presumed to be the slack bus Vθ, therefore there are m - 1 equations for the active power of PV and PQ buses, with m - 1 = N_{PV} + N_{PQ}, and n - 1 equations for the reactive power of PQ buses, with n - 1 = N_{PQ}. ΔP(x) and ΔQ(x) represent the active and reactive power mismatches [32, 46].

So, now the linearised equation 3.36 can be rewritten for the power flow equations as

$$\begin{bmatrix} \Delta P(x_v) \\ \Delta Q(x_v) \end{bmatrix} + J(x_v) \begin{bmatrix} \Delta \theta_v \\ \Delta V_v \end{bmatrix} = 0 \tag{3.42}$$

where the Jacobian matrix $J(x)$ is described by

$$J(x) = \begin{bmatrix} \frac{\delta P_i(x)}{\delta \theta_k} & \frac{\delta P_i(x)}{\delta |V_k|} \\ \frac{\delta Q_i(x)}{\delta \theta_k} & \frac{\delta Q_i(x)}{\delta |V_k|} \end{bmatrix} \tag{3.43}$$

And as the matrices $\frac{\delta P}{\delta \theta}$ and $\frac{\delta Q}{\delta |V|}$ are quadratic so it is the Jacobian matrix $J(x)$ [32, 46].

By the usage of this method, all the values of the collector system can be obtained and analyzed. An essential indicator of a correct design of the collector system are the power losses. In order to obtain the magnitude of these, the sign properties of power generation and demand are used, whereby the sum of active power generated by the wind turbines and collected at the substation, or slack bus, P_0 is calculated. The power losses P_{losses} can be written as

$$P_{losses} = \sum_{i=1}^{n_{WT}} P_i + P_0 \tag{3.44}$$

where n_{WT} is the number of wind turbines in the wind farm. Sedighi et al. exposes in [51] that the active power losses are normally seized as a 2% of the total OWPP capacity.

Conclusively, all required formulas for the calculation and analysis of the power flow in the wind farm are presented.

3.4 Cost Models

The cost of a power plant is typically divided inoto CAPEX and OPEX, yet, the actual price also depends on subsidies, taxes or fuel price [52].

In order to evaluate the costs of the design cost models are required. This section presents firstly a cost model for the cables, and afterward a cost model for energy losses.

3.4.1 Cost of Cables

The design of offshore wind farms is largely driven by Capital Expenditure (CAPEX) [53] since it embraces the cost of the wind turbines, the collection system and the substation. In this thesis, as the wind turbines and the substation remain the same in the different cases are not taken into account.

For OWPP, XLPE cables are usually used. Their manufacturing cost is not easy to assess in pre-feasibility studies. Moreover, transport and installation costs depend on distance from shore, especially from industrial ports, and on seabed kind [54].

The specific cost $C_{c,AC}$ per kilometer length of the AC cables, is based on the rated power S_{rated} [55] and can be calculated by

$$C_{c,AC} = K_1 + K_2 exp^{\left(\frac{K_3 S_{rated}}{10^8}\right)} \qquad \text{[SEK/km]} \tag{3.45}$$

where

$$S_{rated} = \sqrt{3} V_{rated} I_{rated} \tag{3.46}$$

with K_1, K_2 and K_3 as cost constants dependants on the voltage rating, some values can be seen in the Table 2.

Rated voltage [kV]	K_1 [10^6]	K_2 [10^6]	K_3
22	0.284	0.583	6.15
33	0.411	0.596	4.1
45	0.516	0.612	3
66	0.688	0.625	2.05
132	1.971	0.209	1.66
220	3.181	0.11	1.16

Table 2: Cost parameters for AC cables, for different voltages [55].

In view of the fact that the result obtained from the equation 3.45 is per kilometer length of cable, it has to be multiplied by the length of each cable section l_k, which is the euclidean length of the vector between the wind turbine i and wind turbine k or either the last wind turbine of the feeder and the substation. The number of cable sections in an OWPP collector system is indicated as n_{sec}. Hence, the total investment required in cables of the collector system is the sum of the cost of each cable section k.

$$C_{cables} = \sum_{k=1}^{n_{sec}} l_k C_{c,AC}^k \tag{3.47}$$

3.4.2 Cost of Energy Loss

Every design has its specific power losses. These losses can be listed as lost income owing to the impossibility of selling the electricity produced to the electric grid since it could not be exported. It can be seen as fictional cost, related to Operational Expenditure (OPEX) which is normally annualized cost with the unit €/MWh (kWh) [52]. As the cost due to the energy loss are taking for the whole life time, the annual energy loss is computed presuming Full Load Hours (FLH) of the offshore wind farm.

$$E_{loss} = p_{losses} S_{base} FLH \tag{3.48}$$

Once the energy loss is calculated, it has to be multiplied by the electricity price C_{el} of an OWPP. In order to take into account the lost income in a period of time, it has to be discounted of the present value by the discount rate r. So, the Net Present Value (NPV) of the cost of energy loss for the whole life time n_{life} can be computed by

$$NPV_{loss} = E_{loss} C_{el} \sum_{t=0}^{n_{life}} (1+r)^{-t} \tag{3.49}$$

The economic and operational parameters of Table 3 can be found in [56] taken from Cristoph's Research Assingment [10]. For the discount rate r the real Weighted Average Cost of Capital (WACC) is used, which is adjusted for inflation. Since the revenue obtained by selling electricity is tough to estimate, the Levilized Cost of Electricity (LCoE) is taken as a minimum electricity price to break-even with cost and it is presumed to be constant. In such a way, the change in power losses and cable investment can be neglected in front of LCoE. As a percentage of LCoE, OPEX makes up a considerably higher portion for offshore project than onshore [52].

$WACC_{real}$	LCoE Wind Offshore	Full load hours
4.8 %	0.1376 / €kWh	3200

Table 3: Economic parameters based on [56].

4 Methodology

The objective of this thesis is to obtain an optimization of the collection grid of three scales of OWPP. This analysis is performed as in [10], where firstly, in the Reference design, the array-cables laid in the seabed can have any size between the stipulated by the manufacturer [18], being only confined by the ampacity of it, meanwhile, in the Optimized design, the reduction of power losses and investment required drive the election of the cable size.

Firstly, the theoretical background of the optimization by the usage of multi-objective function and the Pareto Front is described. Further, the application for cable sizing is presented. And latter the previous work, as the base case drawn from Cristoph Kaufmann's Research Assignment and two methods for enlarging the wind farm, with a view to the case study are introduced.

4.1 Optimization

By the use of the Newton-Raphson Method, the power flow in the collector system is computed, the electrical viability is checked and the power losses are calculated. Therefore, all the technical part is examined but the economic feasibility needs to be taken into account in order to obtain the techno-economic optimum. The simultaneously and systematically optimization of these objectives is addressed by Multi-Objective Optimization (MOO) [57].

4.1.1 Multi-objective Optimization and the Pareto Front

The optimization process allows the finding of the optimal value or the best solution. Problems with more than one objective are referred to as multi-objective optimization problems, which can be found in everyday life, such as engineering, social studies, economics, and many others [58]. The aim of using the MOO is the simplification of the optimization problem since it does not require complicated equations.

It is important to differentiate the two phases in which the solution of a multi-objective optimization problem can be divided: the optimization of the objective functions involved and the process of deciding what kind of trade-offs are appropriate from the decision maker perspective. Focusing on the way each method deals with the two problems of searching and making decisions one of the most popular classification of MOO techniques is derived [57, 59, 60]:

- *A priori* articulation of preferences (decide $\Rightarrow$ search) : weighted global criterion method, weighted sum method, weighted min-max method, goal programming method and bounded objective function method are some of the techniques following this criteria.
- *A posteriori* articulation of preferences (search $\Leftarrow$ decide) : physical programming, the ϵ-constraint method and normal boundary intersection (NBI) method are some of the techniques following this criteria.
- Progressive articulation of preferences (decide $\Leftrightarrow$ search) : Nash arbitration and objective product method and Rao's method are some of the techniques following this criteria.

Where preferences refer to a decision maker's opinions concerning points in the criterion space.

A different kind of approach is represented by Evolutionary Algorithms that are based on Darwin's theory of survival of the fittest. They are found on the idea that as the population evolves in a genetic algorithm, solutions that are non-dominated are chosen to remain in the population [60].

Mathematically, MOO problems can be defined as [58, 60, 61, 62] :

$$min/max \quad f(x) \;=\; (f_1(x),\, f_2(x), ..., f_p(x)) \tag{4.1}$$

$$\text{subject to:} \quad x \;\in\; U$$

where $x = (x_1, ..., x_n)$ is an n-dimensional decision variable vector, p is the number of objective functions ($p \geq 2$) where $f_p(x)$ is the pth objective function, U is the feasible set and min/max represents the object operation of either minimizing or maximizing.

Since for every x solution in the decision variable space there is a point on the objective function space, the convexity of the solution space and the objective function space is crucial in determining the problem-solving algorithm as if the problem is convex, meaning that all the objective functions and solution area are convex, there are many algorithms useful for solving the problem. The objective function is convex if satisfies equation 4.2 [63] with $\lambda \in [0,1]$. The equation can be better understood by Figure 15, where the line joining the points (x,$f(x)$) and (y,$f(y)$) is above the graph.

$$f(\lambda x + (1-\lambda)y) \;\leq\; \lambda f(x) + (1-\lambda) f(y) \tag{4.2}$$

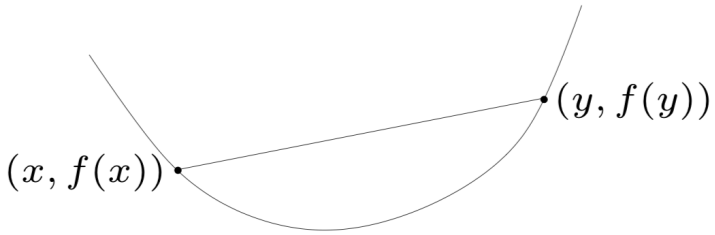

Figure 15: Convex function.

Multi-objective optimization problems are usually defined by measures of performance, also known as objectives, which may be (in)dependent and/or non-commensurable; normally the multiple objectives being optimized conflict [62]. Conversely to single-objective optimization problem, in multi-objective optimization problems there is no single global solution, and it is often necessary to determine a set of points that all fit a predetermined definition for an optimum. The key to defining a set of solutions is the Pareto Optimality Theory, which is applied if the desired set of solutions and objectives indicators are independent and produce a compromise solution.

The concept of Pareto Dominance is mathematically defined as:

A vector **u** = (u_1, ... , u_p) is said to dominate **v** = (v_1, ... , v_p) *if* and *only if* **u** is partially less than **v**, i.e., $\forall i \in \{1, ..., p\}, u_i \leq v_i \wedge \exists i \in \{1, ..., p\} : u_i < v_i$

The concept of Pareto Optimality is mathematically defined as:

A solution $x_u \in U$ is said to be Pareto optimal *if* and *only if* there is no $x_v \in U$ for which $v = f(x_v) = (v_1, ..., v_p)$ dominates $u = f(x_u) = (u_1, ..., u_p)$.

The dominance solution and optimal value in MOO are achieved when one objective function cannot be further optimized (increased) without affecting (reducing) the other objective function, when the Pareto optimality is validated. The set of optimal solutions in MOO is called Pareto optimal solution.

Firstly, some terms in the Pareto optimal solution need to be noted:

- Anchor point: can be obtained through the best of an objective function.
- Utopia point: can be obtained through the intersection of the max/min value of and objective function and the max/min value if the other objective function.

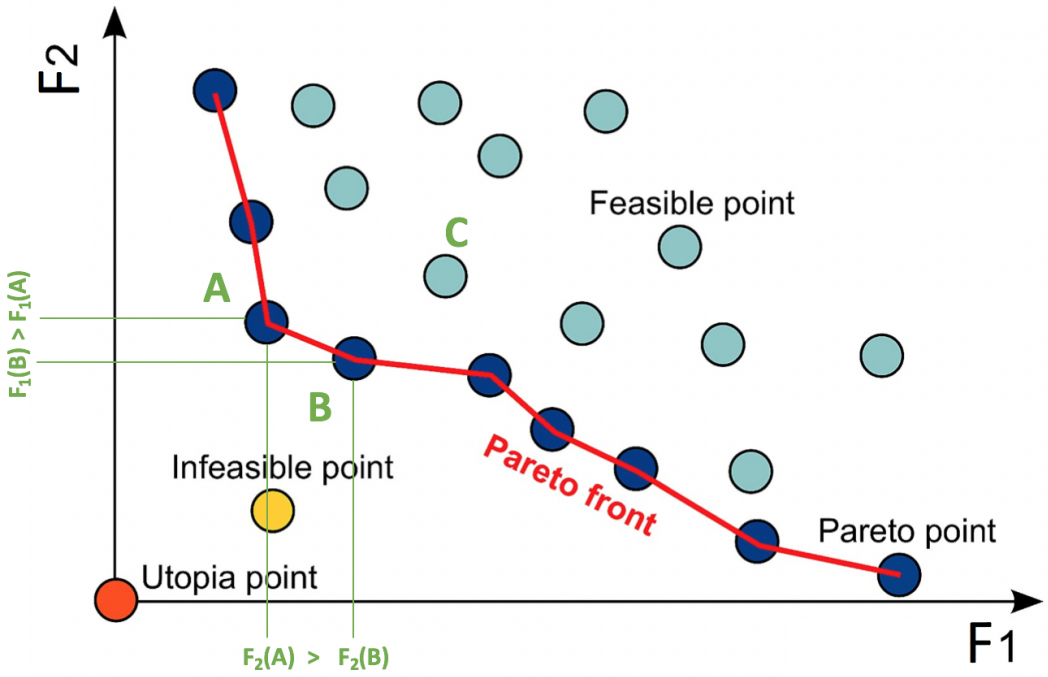

Figure 16: Pareto front [64].

With the help of Figure 16 a descriptive explanation of the Pareto Optimality Theory is done. The axes stand for the two conflicting objectives , each feasible point is plotted as a light blue circle meanwhile the non-feasible points are represented by the yellow circle. The utopia point noted above is here plotted in the cross of the axes. The points A and B dominate the point C, therefore the point C is not in the Pareto front, here indicated by the line in red. On the other hand, the points A and B do not dominate each other as the image of point B is bigger when considering only F_1 objective function and the image of point A is bigger when considering only F_2, hence they belong to the Pareto front.

The scalarization method reduces the multi-objective function into a single-objective one by incorporating scalar fitness functions into the multi-objective functions. This method is also known as linear combination of weights and can be expressed as [58]

$$f(x) \quad = \quad w_1 f_1(x) + w_2 f_2(x) + ... + w_p f_p(x) \tag{4.3}$$

The solution of the fitness function $F(x)$ is determined by the weight w_p of an objective function f_p and display the performance priority. A larger weight represent a higher priority to the objective function which is paired with compared to the ones with smaller weights. There are three different ways to determine the weights [58]:

- Equal weight: gives the same weight to each objective function.

  $w_i = \frac{1}{p}$ where i = 1,2, ... , p and p is the number of objective functions.

- Rank order centroid (ROC) weights: gives ranks using ROC method.

  $$w_i = \frac{1}{p} \sum_{p}^{k=i} \frac{1}{k}$$

- Rank-sum (RS) weights: gives weights in a proportional way.

  $$w_i = \frac{2(p+1-i)}{p(p+1)}$$

4.1.2 Formulation of the Multi-objective Function for Cable Sizing

This thesis puts forward a cable sizing method taking into consideration technical and economical aspects, which should give a different solution if the method applied is the conventional method of cable sizing governed by the ampacity. The cost models for the cables described in Section 3.4.1, and the cost models for energy loss described in Section 3.4.2, can be compared as the two have the same dimension and rely upon the cable diameter. A decision on the cable diameter will affect the ampacity as well as the power losses, and both should be minimized. Implementing the scalarization method, the multi-objective function is reduced to a single-objective function, with the aim to get the Pareto front.

This optimization problem can be classed as a mixed-integer non-linear programming with non-linear constraints, and can be expressed as

$$min\ \{\, C^f_{cable} + NPV^f_{loss} \,\} \tag{4.4}$$

$$min\ \{\, w_1 \cdot C^f_{cable} + w_2 \cdot NPV^f_{loss} \,\} \tag{4.5}$$

$$\text{subject to:} \quad f \in F$$

$$n^f_{\varnothing} \leq 3 \ \wedge \ A^f_{\varnothing} \in A^{man}_{\varnothing}$$

$$I_k \leq I^{amp}_k \ \ \forall \ \ k \in n_{sec}$$

$$\Delta v \leq 5\%$$

$$w_1 + w_2 = 1 \ \ \forall \ \ w_1, w_2 \in [0, 1]$$

where f is a feasible solution inside the feasible solutions set F. The first constraint is referred to the cable diameter, the number of different cable diameters ($n^f_{\varnothing}$) contemplated for a solution should be equal or more than 3 and the set of cable diameters for the feasible solution f ($A^f_{\varnothing}$) has the cable diameter given by the manufacturer ($A^{man}_{\varnothing}$). The next constraint considers the maximum current a cable can carry continuously under the conditions of use without exceeding its temperature rating by limiting the current (I_k) flowing through a cable section k to the ampacity from that section of cable (I^{amp}_k). The next constraint restricts the voltage drop (Δv) between each WT and the substation to equal or less a 5%. Finally, the latter constraint reflects the weighting concept, where the sum of the weighting factors (w_1, w_2) needs to be equal to 1 while both factors are between the values 0 and 1, meaning that there is no priority for any objective. A solution is considered as feasible if the second and the third constraint are satisfied.

The first minimization function 4.4 regards the general objective of minimizing the sum of both costs, cable cost and energy loss cost. Meanwhile, the idea of Pareto efficiency is applied to the second minimization function 4.5 in order to find the optimal solutions with the usage of the weighting factors.

4.2 Preliminary Work

As said in Section 2.2 the understanding of Cristoph Kaufmann's Research Assignment is an essential step. Therefore in this section, at first, the offshore wind farm arrangement is presented and all input parameters for the design are listed, obtained from [10]. Next, the two designs are presented and taken as grounding results for the first case study and lastly two methods for enlarging the offshore wind farm are suggested.

A generic symmetric design of the offshore wind farm is embraced from [65]. The offshore wind turbine selected is the wind turbine Siemens Gamesa SWT-6.0-154 [66]. The analysis of reactive power has been discussed in other studies as [28, 43] therefore, a power factor of $\cos\phi = 1$ is assumed. The substation is settled in proximity outside the array. This research considers the static case of 100% load on the cable. Likewise, the losses throughout the transformer and cables of the wind turbine are neglected as well as the wake losses and distribution of wind speeds.

Parameter	Value
Number of wind turbines	49
Topology	7x7
Horizontal spacing	7D
Vertical spacing	9D
Wind turbine model	Siemens Gamesa SWT-6.0-154 [66]
Rated power	6MW
Rotor diameter	154m
OWPP capacity	294MW
$n_{\varnothing}^{f}$	3 different cable diameters
Full load hours	3200h
Rated Voltage	33kV
$\cos\phi$	1
Cable diameters	see Table 5
Cost of cable	see equation 3.45, depending on ampacity
LCoE	0.1376€/kWh
$WACC_{real}$	4.8%
Life time	20 years
Base apparent power (S_{base})	100MW

Table 4: Assumptions for the optimization [10].

Cross-section	Conductor Diameter	Insulation Thickness	Ampacity	Capacitance	Charging Current per phase at 50Hz	Inductance
mm^2	mm	mm	A	mF/km	A/km	mH/km
95	11.2	8	300	0.18	0.10	0.44
120	12.6	8	340	0.19	0.10	0.42
150	14.2	8	375	0.21	0.11	0.41
185	15.8	8	420	0.22	0.12	0.39
240	18.1	8	480	0.24	0.13	0.38
300	20.4	8	530	0.26	0.14	0.36
400	23.2	8	590	0.29	0.16	0.35
500	26.2	8	655	0.32	0.17	0.34
630	29.8	8	715	0.35	0.19	0.32
800	33.7	8	775	0.38	0.21	0.31

Table 5: XLPE three-core copper submarine cable parameters for 30 kV (U_m=36 kV) from the manufacturer ABB [18].

There are two types of designs, the first one called Reference design represents the array cables of the OWPP selected by the only restriction of enough ampacity of the cable to carry the current generated by the wind turbines. The latter named Optimized design, as the name says, represents the array cables of the OWPP selected by the usage of the proposed optimization method described previously to this section.

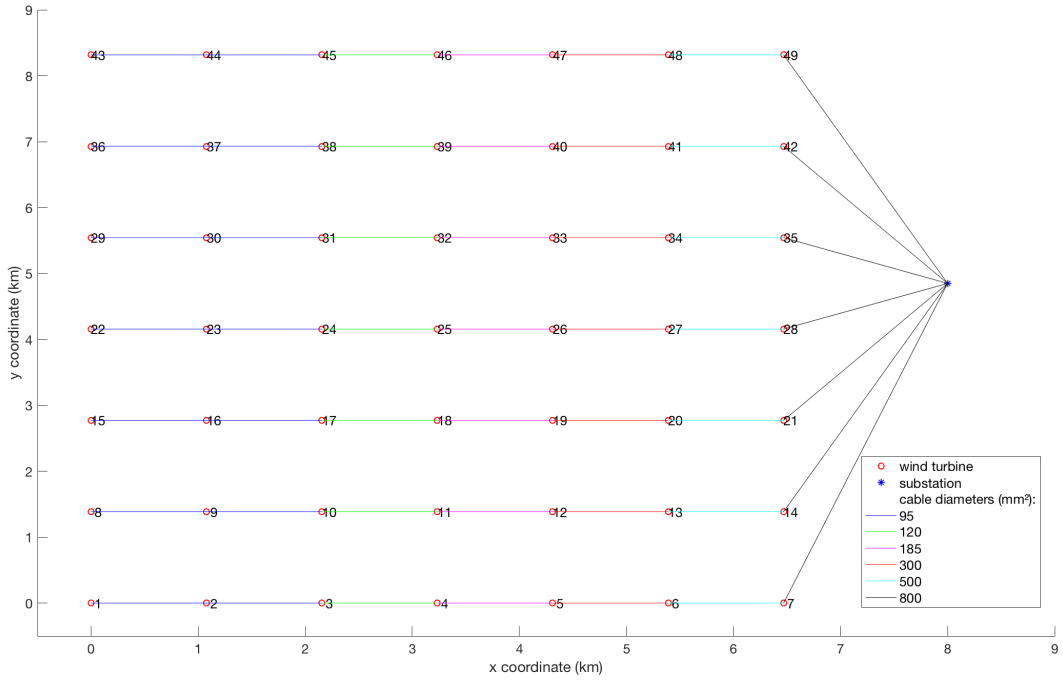

Figure 17: Reference wind farm: cable diameter and wind farm layout.

Set of cables	[95 120 185 300 500 800]
Total cost of cables	20.1304 M€
Relative power losses	1.1128%
Annual energy losses	10.4693 GWh
Total cost of energy losses	19.7447 M€
Sum of total costs	39.8751 M€

Table 6: Results from the Reference design [10].

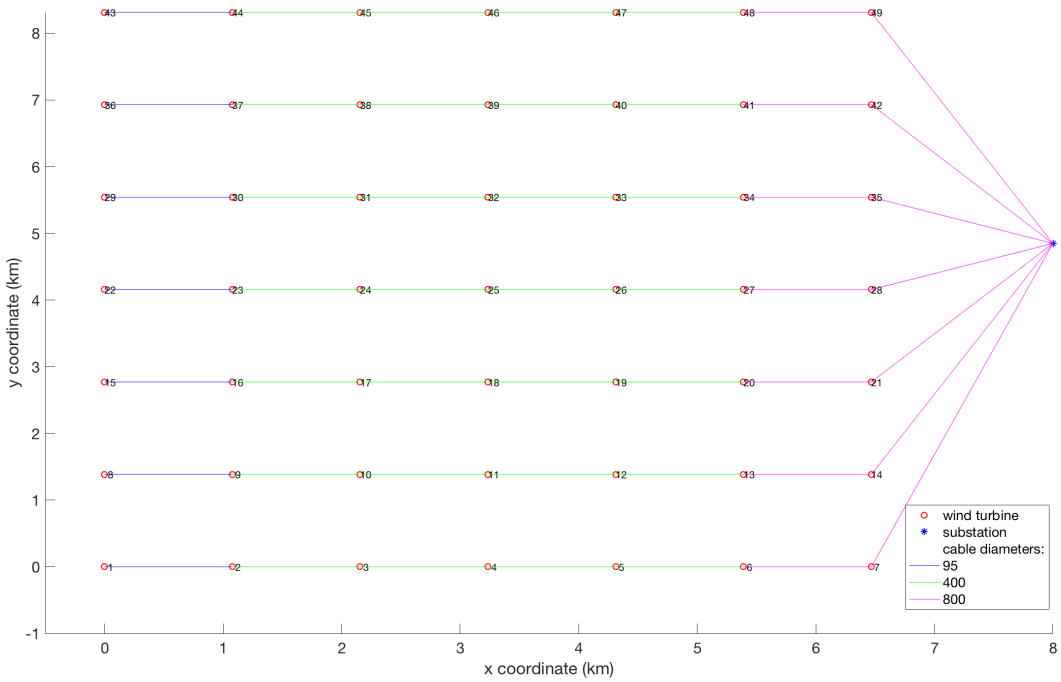

Figure 18: Optimized wind farm: cable diameter and wind farm layout.

Set of cables	[95 400 800]
Total cost of cables	23.6515 M€
Relative power losses	0.81375%
Annual energy losses	7.6558 GWh
Total cost of energy losses	14.4385 M€
Sum of total costs	38.09 M€
Total time to calculate all feasible solutions	1453.1476 seconds

Table 7: Results from the Optimized design [10].

With the aim of enlarging the wind farm, two methods can be applied. The first one consists on adding wind turbines to the string-feeders of the actual design, since the maximum cable ampacity of the cables for 30kV from the manufacturer ABB [18] is 775 A with a cross-section of 800 mm^2 and just by adding one wind turbine to the string-feeder the last section of cable needs to carry 839.76 A, hypothetical cable parameters are used for this analysis based on the cables for 45kV from the manufacturer ABB [18]. The second method, is adding string-feeders to the actual design, since the number of wind turbines in a string-feeder does not change the same cables from the basis design can be used, with the parameters listed in Table 5.

Adding one wind turbine to each string-feeder

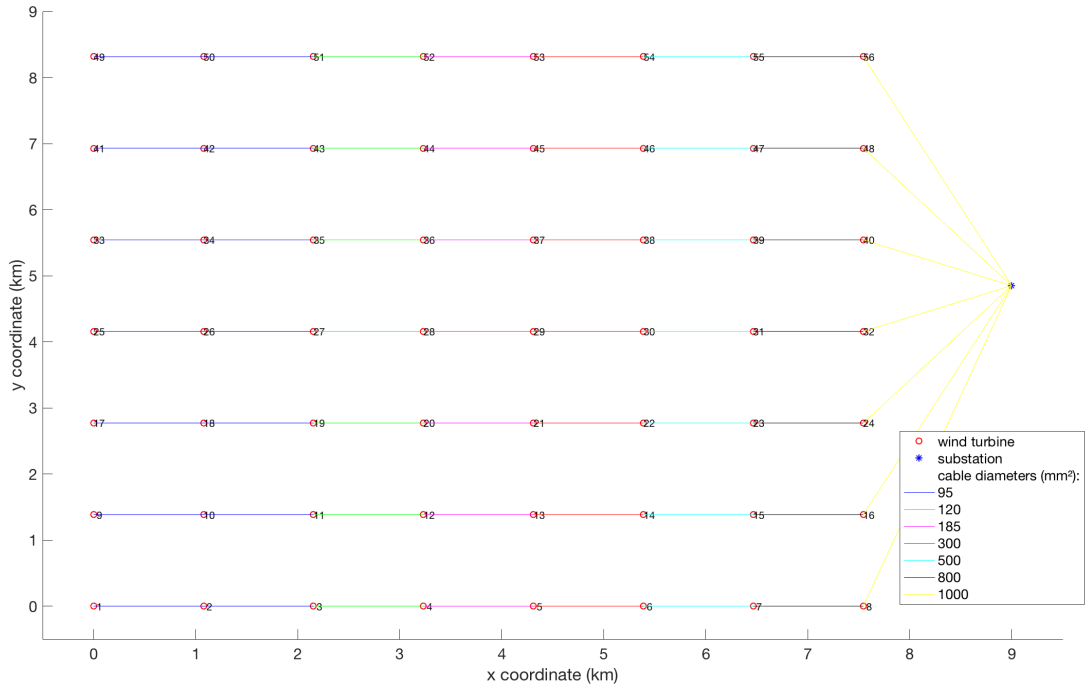

Figure 19: Reference wind farm with one wind turbine more by string-feeder: cable diameter and wind farm layout.

Set of cables	[95 120 185 300 500 800 1000]
Total cost of cables	24.7865 M€
Relative power losses	1.1498%
Annual energy losses	12.3626 GWh
Total cost of energy losses	23.3153 M€
Sum of total costs	48.1018 M€

Table 8: Results from the Reference design with one wind turbine more by string-feeder.

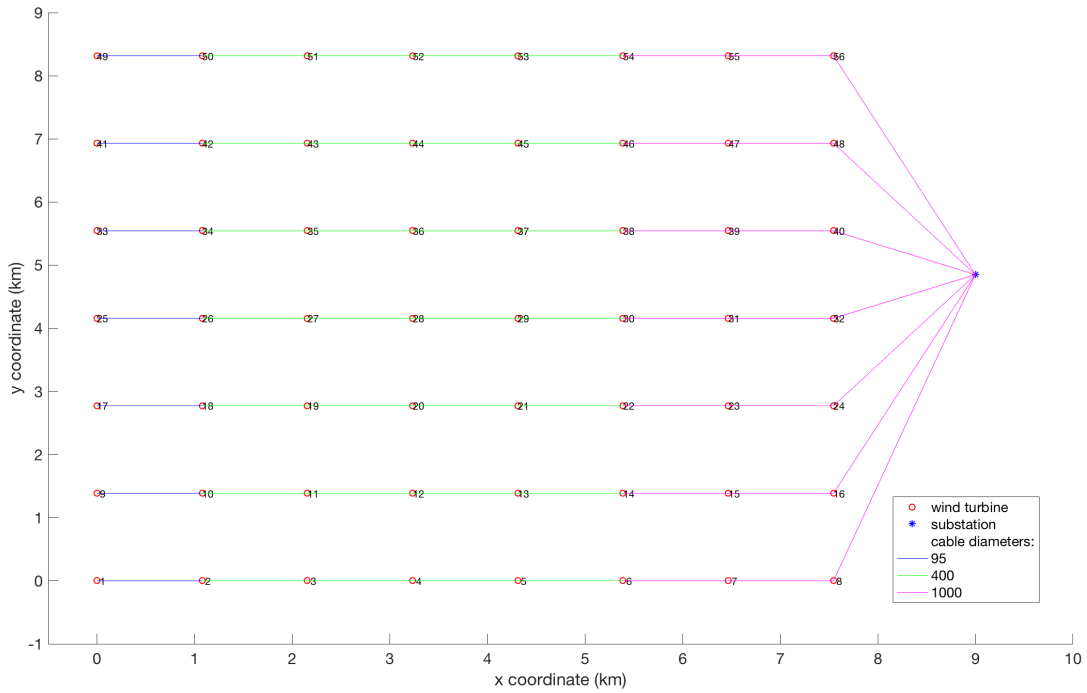

Figure 20: Optimized wind farm with one wind turbine more by string-feeder: cable diameter and wind farm layout.

Set of cables	[95 300 1000]
Total cost of cables	29.3139 M€
Relative power losses	0.86365%
Annual energy losses	9.286 GWh
Total cost of energy losses	17.513 M€
Sum of total costs	46.8269 M€
Total time to calculate all feasible solutions	63104.7989 sec

Table 9: Results from the Optimized design with one wind turbine more by string-feeder.

The optimization implies a cable investment of 4.53 M€, which represents an increase of 18.27%. But, with a reduction on the relative power losses of 0.29% a decrease on the annual energy losses of 3.08 GWh or 24.89% is performed. The overall picture can be taken from the sum of both costs, considering the cost of energy loss as operational cost as well as the investment in cables, the Optimized design results in 1.27 M€on savings or a reduction of 2.65% of the investment required.

Design	Set of cables	Relative power losses (336 MW capacity) %	Annual energy losses GWh	Total cost of energy losses M€	Total cost of cables M€
Reference	95 120 185 300 500 800 1000	1.15	12.36	23.32	24.79
Optimized	95 300 1000	0.86	9.29	17.51	29.31

Table 10: Comparison of key values of the Reference and the Optimized design with one wind turbine more by string-feeder.

Adding one string-feeder

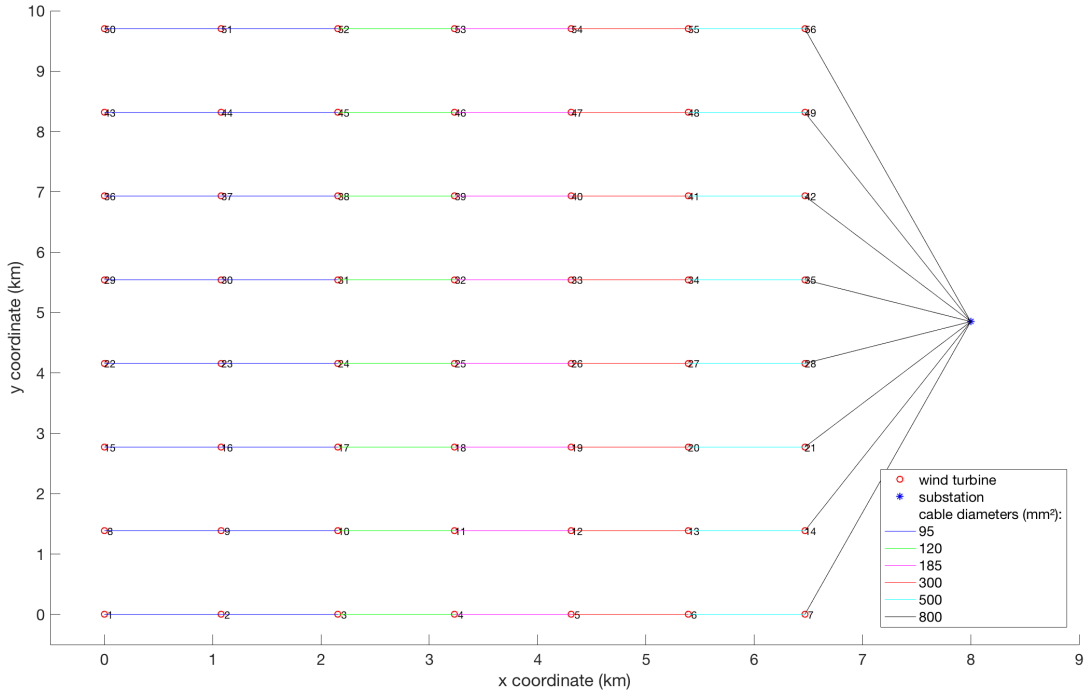

Figure 21: Reference wind farm with one string-feeder more: cable diameter and wind farm layout.

Set of cables	[95 120 185 300 500 800]
Total cost of cables	23.9367 M€
Relative power losses	1.1472%
Annual energy losses	12.3352 GWh
Total cost of energy losses	23.2637 M€
Sum of total costs	47.2004 M€

Table 11: Results from the Reference design with one string-feeder more.

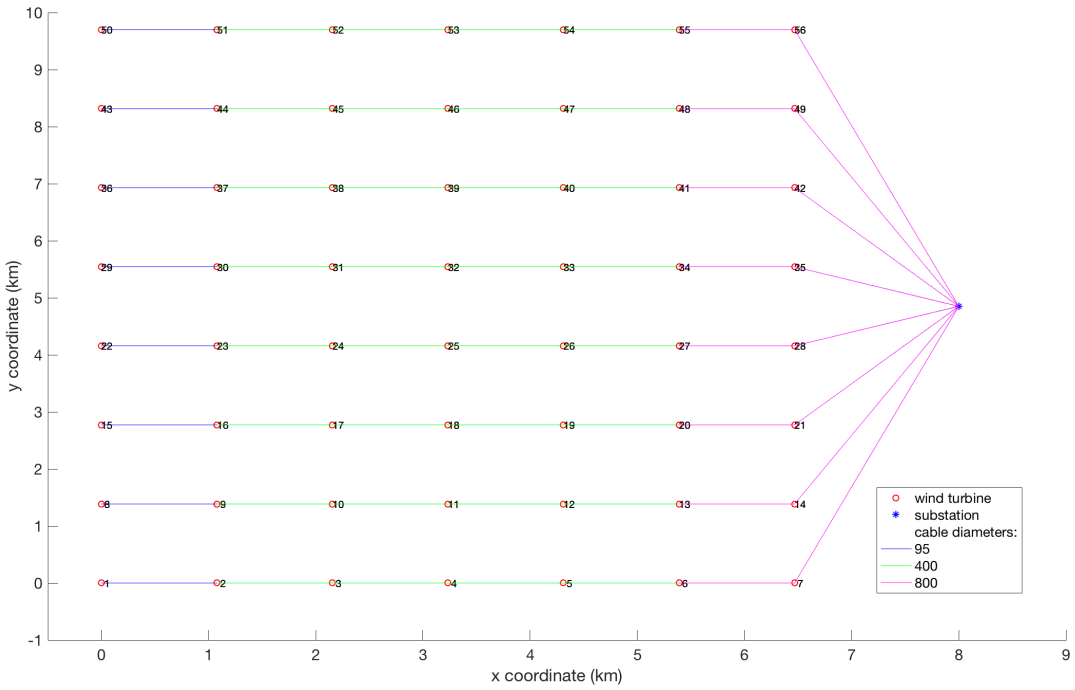

Figure 22: Optimized wind farm with one string-feeder more: cable diameter and wind farm layout.

Set of cables	[95 400 800]
Total cost of cables	28.1112 M€
Relative power losses	0.85416%
Annual energy losses	9.1839 GWh
Total cost of energy losses	17.3205 M€
Sum of total costs	45.4318 M€
Total time to calculate all feasible solutions	487.3108 seconds

Table 12: Results from the Optimized design with one string-feeder more.

The optimization implies a cable investment of 4.18 M€, which represents an increase of 17.44%. But, with a reduction on the relative power losses of 0.29% a decrease on the annual energy losses of 3.15 GWh or 25.55% is performed. The overall picture can be taken from the sum of both costs, considering the cost of energy loss as operational cost as well as the investment in cables, the Optimized design results in 1.77 M€on savings or a reduction of 3.75% of the investment required.

Design	Set of cables	Relative power losses (336 MW capacity) %	Annual energy losses GWh	Total cost of energy losses M€	Total cost of cables M€
Reference	95 120 185 300 500 800	1.15	12.34	23.26	23.94
Optimized	95 400 800	0.85	9.184	17.32	28.11

Table 13: Comparison of key values of the Reference and the Optimized design of the design with one string-feeder more.

With the purpose of enlarging the wind farm, the methods by adding one wind turbine to each string-feeder and adding one string-feeder are presented. As can be seen from Table 10 and from Table 13, enlarging the wind farm by adding string-feeders reduces both the total cost of cables and the total cost of energy losses. So it is correct to assume that the enlarging should be done by this way, but enlarging the wind farm by the first method entails a cable length of 73.70km meanwhile by the second method a cable length of 78.02km which can be traduced into more installation cost and problems. Therefore, in the case study, the first method is applied and following a combination of both in order to get an squared layout.

5 Case Study

This thesis comprehends the study of three different OWPP by changing the number of wind turbines on it. The wind farm layout and the input parameters are taken from [10] but with different cable parameters since the rated voltage is upgraded to 45kV. Therefore the cable parameters are listed in Table 14. As the rated voltage of the collector system is 45kV, each wind turbine injects 76.98 A, calculated with the following equation

$$P_{rated} = \sqrt{3} V_{rated} I \cos\phi \tag{5.1}$$

where P_{rated} is the output rated power of the wind turbine, V_{rated} is the rated power of the collector system and I is the current injected by the wind turbine. The $\sqrt{3}$ is needed since the voltage and the current are referred to the line not to the phase and the system is balanced in current with equal impedance and equal phase angle of the impedance. And $\cos\phi$ represents that this values are complex. Except for I which is the unknown parameter, the rest are listed in Table 4 from Section 4.2.

Cross-section	Conductor Diameter	Insulation Thickness	Ampacity	Capacitance	Charging Current per phase at 50Hz	Inductance
mm^2	mm	mm	A	mF/km	A/km	mH/km
95	11.2	8	300	0.18	1.5	0.43
120	12.6	8	340	0.19	1.6	0.42
150	14.2	8	375	0.21	1.6	0.40
185	15.8	8	420	0.22	1.8	0.39
240	18.1	8	480	0.24	2.0	0.37
300	20.4	8	530	0.26	2.2	0.36
400	23.2	8	590	0.29	2.3	0.35
500	26.2	8	655	0.32	2.6	0.33
630	29.8	8	715	0.35	2.9	0.32
800	33.7	8	775	0.38	3.1	0.31
1000	37.9	8	825	0.42	3.5	0.30

Table 14: XLPE three-core copper submarine cable parameters for 45 kV (U_m=52 kV) from the manufacturer ABB [18].

Each case study has different number of wind turbines, and hence different capacity. At first, the same number of wind turbines, 49 WT, as [10] is implemented. Secondly, the number of wind turbines is incremented by the application of the first method explained in Section 4.2, adding wind turbines to each string-feeder. And lastly, the two methods are combined to obtain a squared offshore wind farm.

For each case, the Reference design and the Optimized design are presented, the results listed and a brief discussion is made. The voltage check for each case study and design can be found in Appendix: Voltage Check.

All calculations are computed and programmed with The MathWorks Inc. software MATLAB_R2108b.

5.1 First Case

In this first case, the wind farm is composed of 49 WT in order to compare the results with the case study from [10].

5.1.1 Reference Design

A cable diameter is given to each section of cables, with the only limitation of enough ampacity of the cable to carry the current through the collector system. The wind farm layout is presented in Figure 23. Five different cable diameters are used for seven sections of cable. It can be seen that the increment in cable diameter does not follow the same rules as the ascending order from the manufacturer from Table 14. This is due to the current injected by each wind turbine is higher than the increase of ampacity, hence some diameters are skipped. The total cable length is 66.47 km and together with the set of cables derive into a total investment on cables of nearly 14 M€. The 0.93% of relative power losses, which is 2.74 MW out of the OWPP capacity of 294 MW, is under the 2% that [51] exposes as regular.

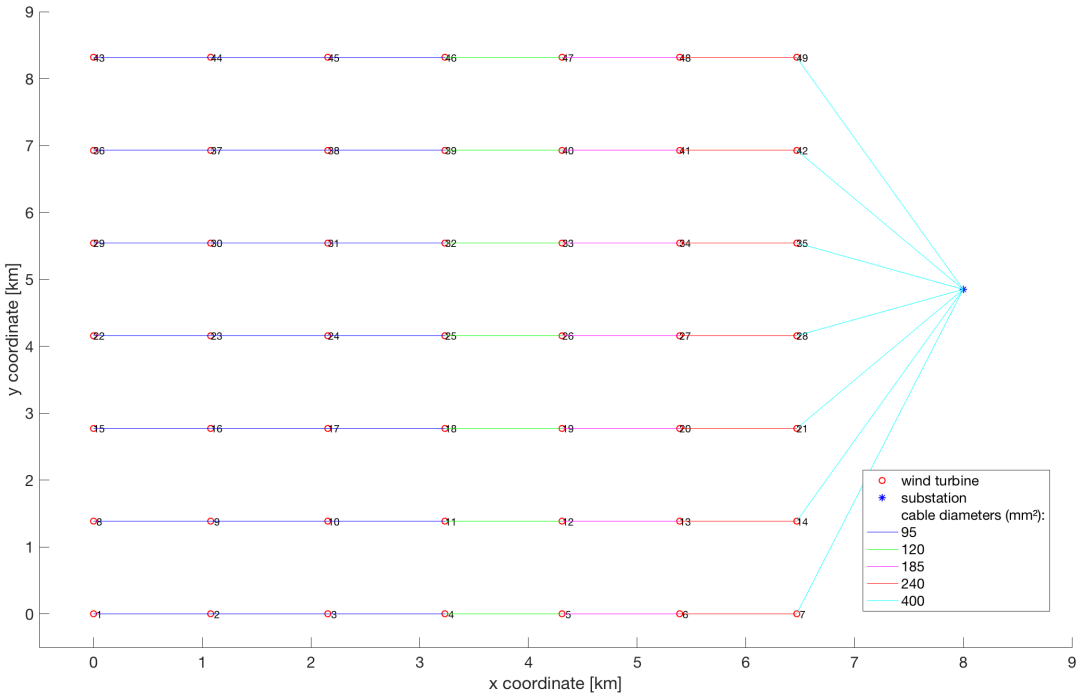

Figure 23: Reference wind farm of the first case study: cable diameter and wind farm layout.

Set of cables	[95 120 185 240 400]
Total cost of cables	13.9998 M€
Relative power losses	0.9306%
Annual energy losses	8.7564 GWh
Total cost of energy losses	16.5109 M€
Sum of total costs	30.5106 M€

Table 15: Results from the Reference design of the first case study.

5.1.2 Optimized Design

In order to achieve a techno-economic optimum, all feasible cable sections combinations are taken into account. As well, each combination has to fulfill the limitation of the ampacity. The Pareto Front of the multi-objective function 4.5 is plotted in Figure 24, each point represents an optimum, or non-dominated solution, where the weight w_i is ranged between 0 and 1 with a step size of 0.0005, so that no specific preference of the decision maker is assumed. It presents a convex shape due to the aim of minimization of the function. It can be seen that the distribution is not equal, there are more feasible solutions at higher cost of cables, meaning larger diameters, than at lower cost of cables with higher cost of energy loss. In other words, the contribution of the cost of cables dominates to the cost of energy loss when both objectives are computed in one single-objective function. Hence, the usage of such a fine step size, as it provides a more non-dominated solution for the Pareto front.

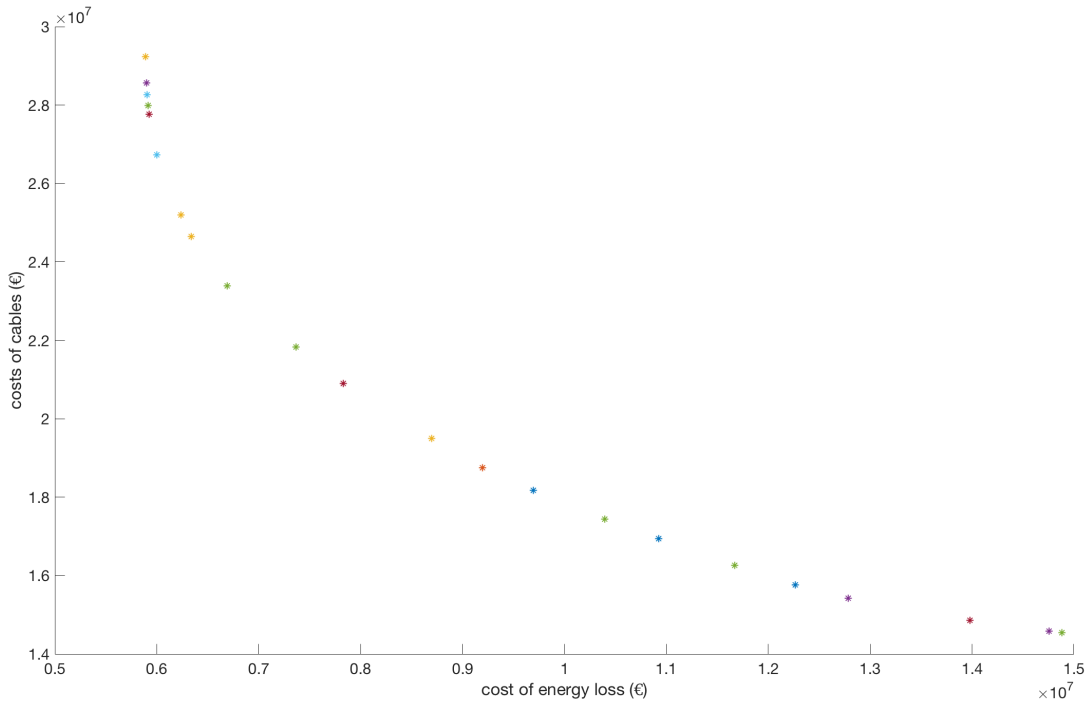

Figure 24: Pareto front of the multi-objective function of the first case study.

Due to the considerably variation of distance between points, a general formulation can not be achieved. Therefore, with the aim of guessing a range where the minimum can be achieved, the sum of the two costs without the weight factors, and with only the combinations from the Pareto front, is plotted against the weight factor w_i of the multi-objective function in Figure 25. The lowest sum of costs is achieved for weights of 0.495 and 0.510 for w_1 with a sum of costs of 27.84 M€.

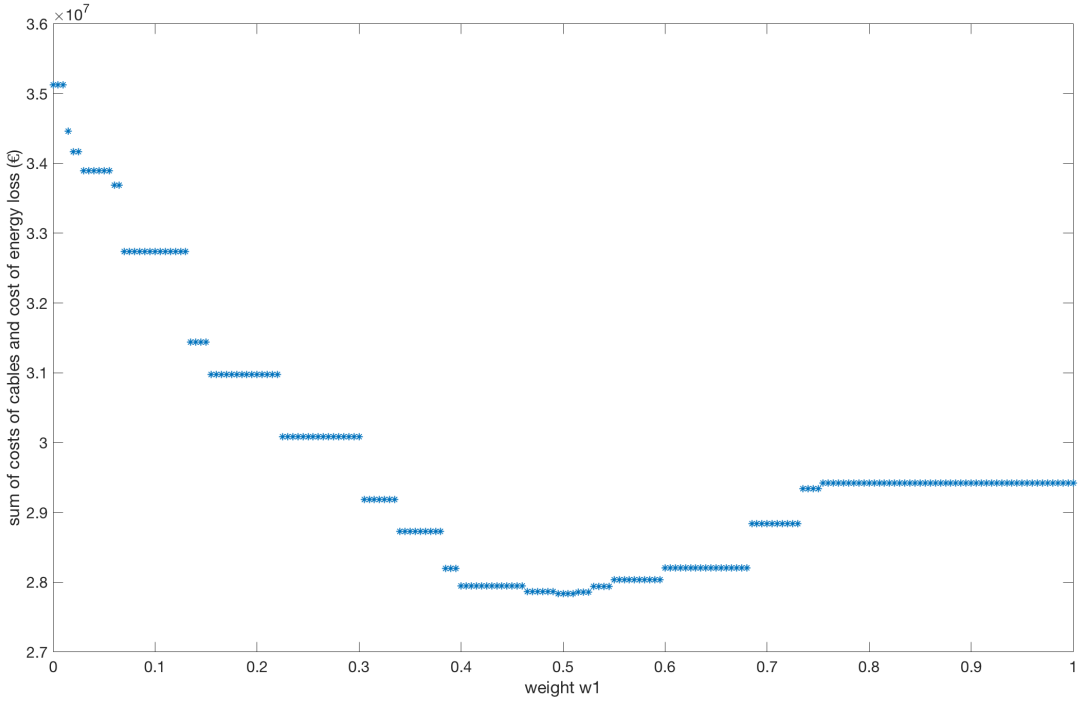

Figure 25: Sum of costs for each optimum depending on the weight factor for the first case study.

The wind farm layout with the optimized cable diameters is plotted in Figure 26, the conjecture before mentioned of the dominance of larger diameter cables is now proven as for the first and second cable sections, between wind turbine 1 and 3, the smallest diameter of 95 mm^2 is chosen, meanwhile for the major number of sections a diameter of 400 mm^2 is assigned even though not being necessary in some sections. And finally, for the last cable section, between wind turbine 7 and the substation, a diameter of 630 mm^2 is designated.

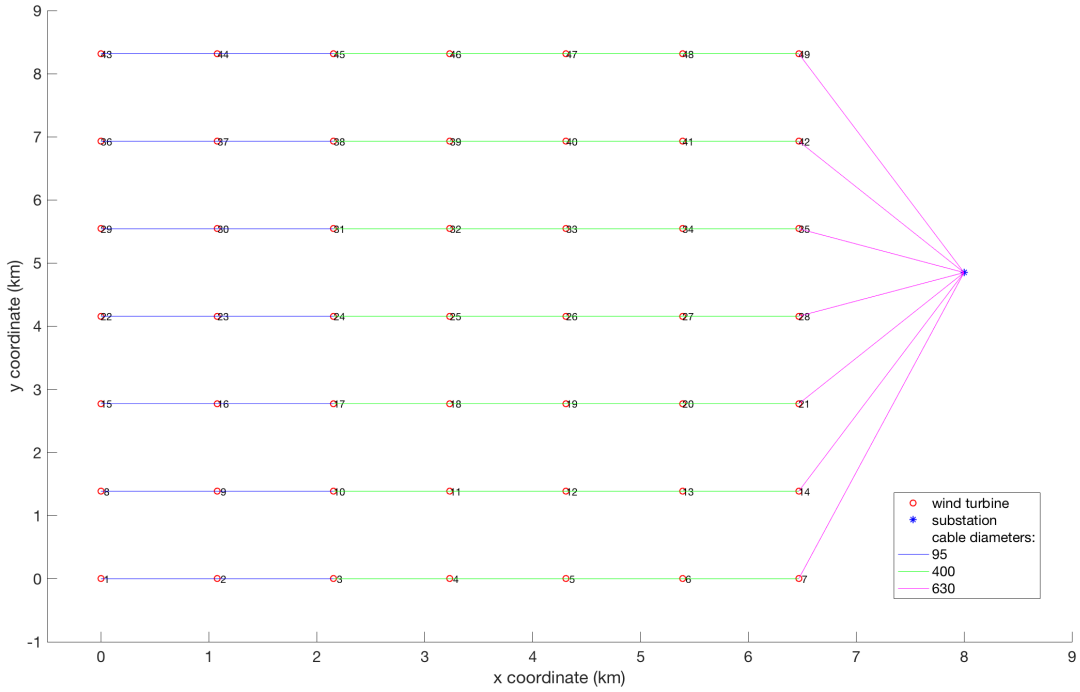

Figure 26: Optimized wind farm of the first case study: cable diameter and wind farm layout.

Set of cables	[95 240 400]
Total cost of cables	18.1697 M€
Relative power losses	0.5464%
Annual energy losses	5.1400 GWh
Total cost of energy losses	9.6939 M€
Sum of total costs	27.8636 M€
Total time to calculate all feasible solutions	598.6348 seconds

Table 16: Results from the Optimized design of the first case study.

5.1.3 Discussion

The optimization implies a cable investment of 4.17 M€, which represents an increase of 29.79%. But, with a reduction on the relative power losses of 0.38% a decrease on the annual energy losses of 3.62 GWh or 41.30% is performed. The overall picture can be taken from the sum of both costs, considering the cost of energy loss as operational cost as well as the investment in cables, the Optimized design results in 2.65 M€on savings or a reduction of 8.68% of the investment required.

Design	Set of cables	Relative power losses (294 MW capacity) %	Annual energy losses GWh	Total cost of energy losses M€	Total cost of cables M€
Reference	95 120 185 240 400	0.93	8.76	16.51	≈ 14
Optimized	95 240 400	0.55	5.14	9.70	18.17

Table 17: Comparison of key values of the Reference and the Optimized design of the first case study.

5.2 Second Case

In this second case, the wind farm is enlarged by having the maximum number of wind turbines in a string-feeder that the cables assumed can carry. This number is 10 wind turbines as it implies a current of 769.80 A and the maximum ampacity available is 825 A for a cross-section of 1000 mm^2 (see Table 14) since an extra wind turbine, 11 WT would increase the current to 846.78 A, which cannot be carried by the available cables.

5.2.1 Reference Design

As in the first case, a cable diameter is given to each section of cables, with the only limitation of enough ampacity of the cable to carry the current through the collector system. The wind farm layout is presented in Figure 27. Eight different cable diameters are used for ten sections of cable. As in the first case study, the increment in cable diameter does not follow the same rules as the ascending order from the manufacturer from Table 14 for the same reason. The total cable length is 88.18 km and together with the set of cables derive into a total investment on cables of 23.29 M€. The 0.99% of relative power losses, which is 4.18 MW out of the OWPP capacity of 420 MW, is under the 2% that [51] exposes as regular.

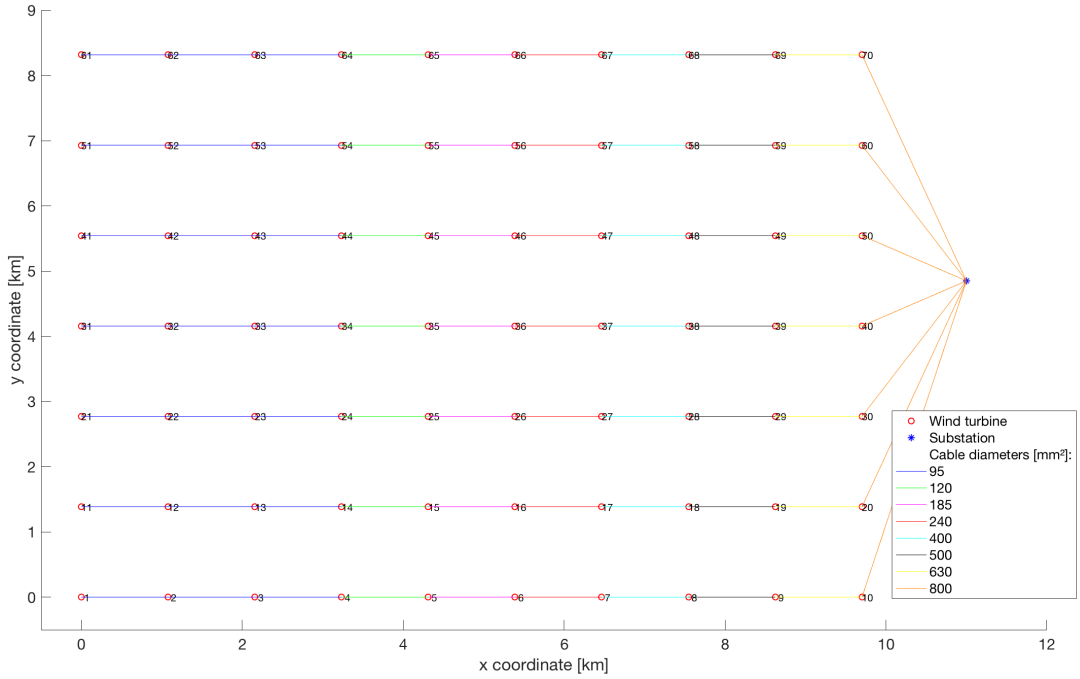

Figure 27: Reference wind farm of the second case study: cable diameter and wind farm layout.

Set of cables	[95 120 185 240 400 500 630 800]
Total cost of cables	23.2930 M€
Relative power losses	0.9948%
Annual energy losses	13.3698 GWh
Total cost of energy losses	25.2150 M€
Sum of total costs	48.5080 M€

Table 18: Results from the Reference design of the second case study.

5.2.2 Optimized Design

As in the first case study, in order to achieve a techno-economic optimum, all feasible cable sections combinations are taken into account. As well, each combination has to fulfill the limitation of the ampacity. The Pareto Front of the multi-objective function 4.5 is plotted in Figure 28, like in the first case study each point represents an optimum, or non-dominated solution, where the weight w_i is ranged between 0 and 1 with a step size of 0.0005, so that no specific preference of the decision maker is assumed. It presents a convex shape due to the aim of minimization of the function. Here, the unequal distribution is more significant, the amount of feasible solutions for larger cable sections is considerably higher than at higher cost of energy loss, meaning smaller cable sections. Therefore the contribution of the cost is notably more dominant to the cost of energy loss when both objectives are computed in one single-objective function. Hence, the usage of such a fine step size is more relevant, as it provides a more non-dominated solution for the Pareto front.

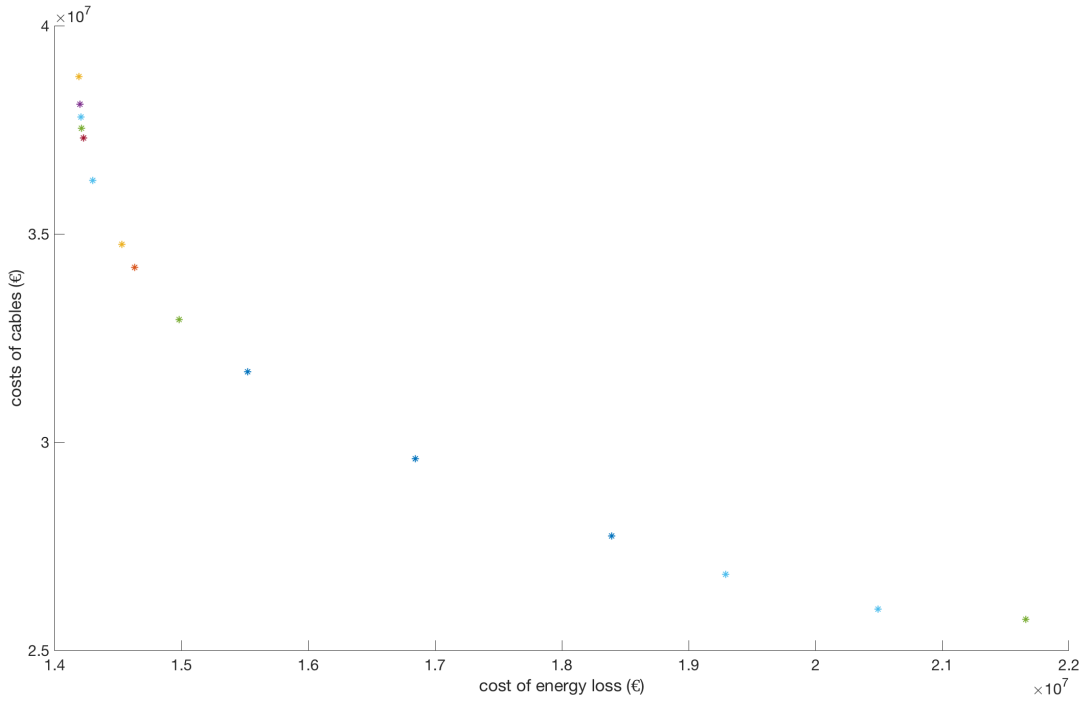

Figure 28: Pareto front of the multi-objective function of the second case study.

Focusing on guessing a range where the minimum can be achieved, the sum of the two costs without the weight factors, and only the combinations from the Pareto front, is plotted against the weight factor w_i of the multi-objective function in Figure 29. The lowest sum of costs is achieved for weights of 0.495 and 0.585 for w_1 with a sum of costs of 46.12 M€.

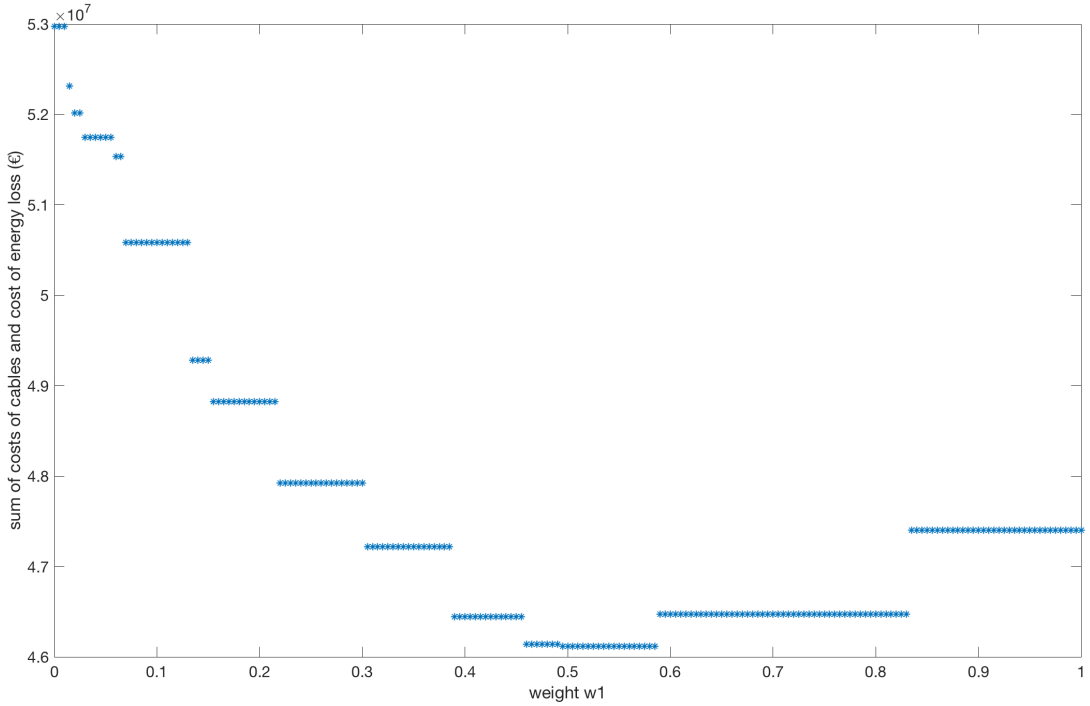

Figure 29: Sum of costs for each optimum depending on the weight factor for the second case study.

The wind farm layout with the optimized cable diameters is plotted in Figure 30, the conjecture before mentioned of the dominance of larger diameter cables is now proven as for the first and second cable sections, between wind turbine 1 and 3, the smallest diameter of 95 mm^2 is chosen, meanwhile for the following four sections, form wind turbine 3 to wind turbine 7, a diameter of 400 mm^2 is assigned even though not being necessary in some sections. And finally, for the lasts sections, from wind turbine 7 to the substation, a diameter of 800 mm^2 is designated.

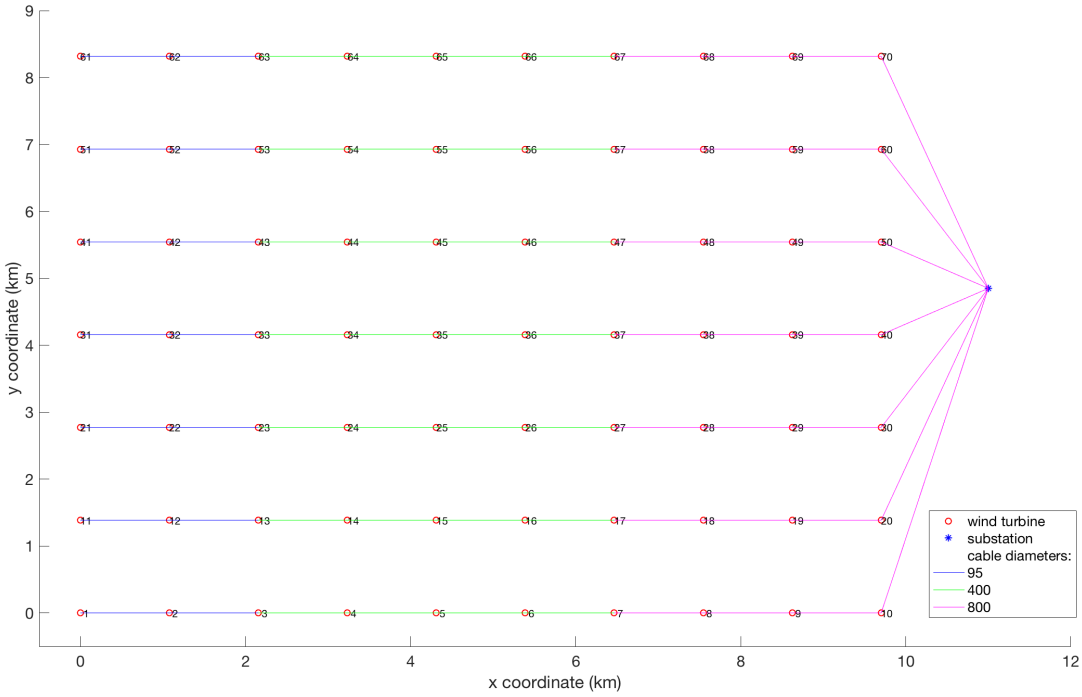

Figure 30: Optimized wind farm of the second case study: cable diameter and wind farm layout.

Set of cables	[95 400 800]
Total cost of cables	27.7474 M€
Relative power losses	0.7257%
Annual energy losses	9.7533 GWh
Total cost of energy losses	18.3943 M€
Sum of total costs	46.1417 M€
Total time to calculate all feasible solutions	1601.5716 seconds

Table 19: Results from the Optimized design of the second case study.

5.2.3 Discussion

The optimization implies a cable investment of 4.45 M€, which represents an increase of 19.12%. But, with a reduction on the relative power losses of 0.27% a decrease on the annual energy losses of 3.62 GWh or 27.05% is performed. The overall picture can be taken from the sum of both costs, considering the cost of energy loss as operational cost as well as the investment in cables, the Optimized design results in 2.37 M€on savings or a reduction of 4.88% of the investment required.

Design	Set of cables	Relative power losses (420 MW capacity) %	Annual energy losses GWh	Total cost of energy losses M€	Total cost of cables M€
Reference	95 120 185 240 400 500 630 800	0.99	13.37	25.22	23.29
Optimized	95 400 800	0.73	9.75	18.39	27.75

Table 20: Comparison of key values of the Reference and the Optimized design of the second case study.

5.3 Third Case

In this third case, the wind farm is enlarged by a combination of both methods explained in Section 4.2, adding wind turbines in each string-feeder and adding string-feeders to the wind farm to get an squared layout. As said in the second case, the maximum number of wind turbines in a string-feeder is 10 WT, therefore three string-feeders are added, getting a wind farm of 100 wind turbines.

5.3.1 Reference Design

As in the previous cases, a cable diameter is given to each section of cables, with the only limitation of enough ampacity of the cable to carry the current through the collector system. The wind farm layout is presented in Figure 31. Eight different cable diameters are used for ten sections of cable. As before, the increment in cable diameter does not follow the same rules as the ascending order from the manufacturer from Table 14 for the same reason. The total cable length is 135.89 km and together with the set of cables derive into a total investment on cables of 37.01 M€. The 1.09% of relative power losses, which is 6.55 MW out of the OWPP capacity of 600 MW, is under the 2% that [51] exposes as regular.

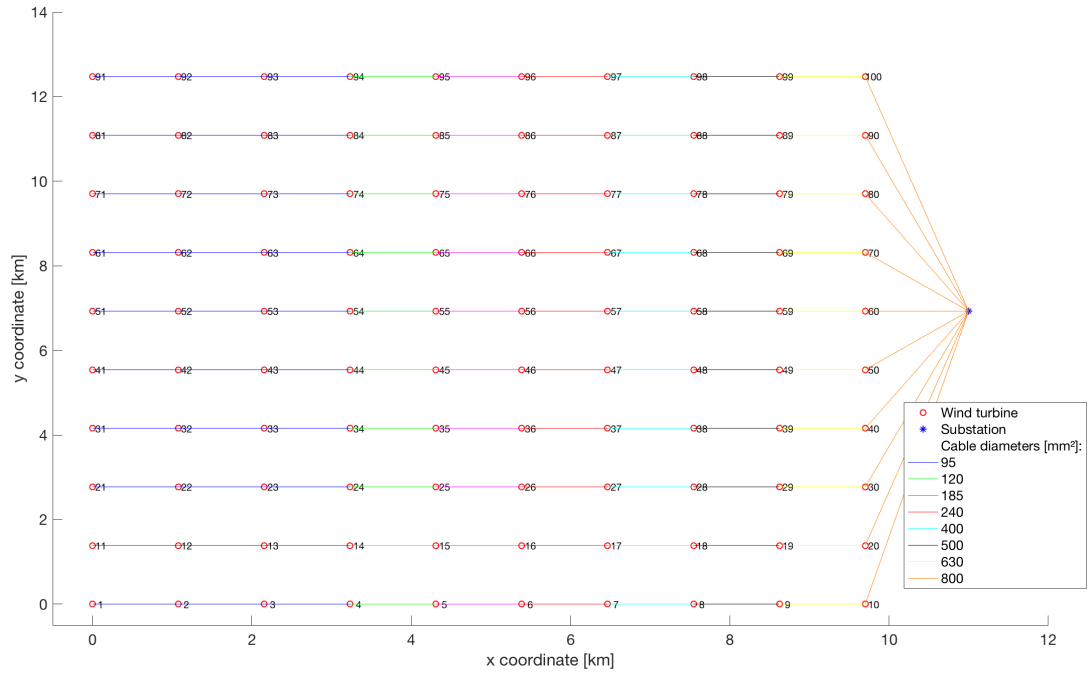

Figure 31: Reference wind farm of the third case study: cable diameter and wind farm layout.

Set of cables	[95 120 185 240 400 500 630 800]
Total cost of cables	37.0102 M€
Relative power losses	1.0917%
Annual energy losses	20.9603 GWh
Total cost of energy losses	39.5303 M€
Sum of total costs	76.5405 M€

Table 21: Results from the Reference design of the third case study.

5.3.2 Optimized Design

Identically to the previous cases, in order to achieve a techno-economic optimum, all feasible cable sections combinations are taken into account. As well, each combination has to fulfill the limitation of the ampacity. The Pareto Front of the multi-objective function 4.5 is plotted in Figure 32, where, as in the former cases, each point represents an optimum, or non-dominated solution, where the weight w_i is ranged between 0 and 1 with a step size of 0.0005, so that no specific preference of the decision maker is assumed. It presents a convex shape due to the aim of minimization of the function. The distribution is uneven as in the earlier cases, but not as much as in the second case. Still, the contribution of the cost is dominant to the cost of energy loss when both objectives are computed in one single-objective function. Hence, the usage of such a fine step size, as it provides a more non-dominated solution for the Pareto front.

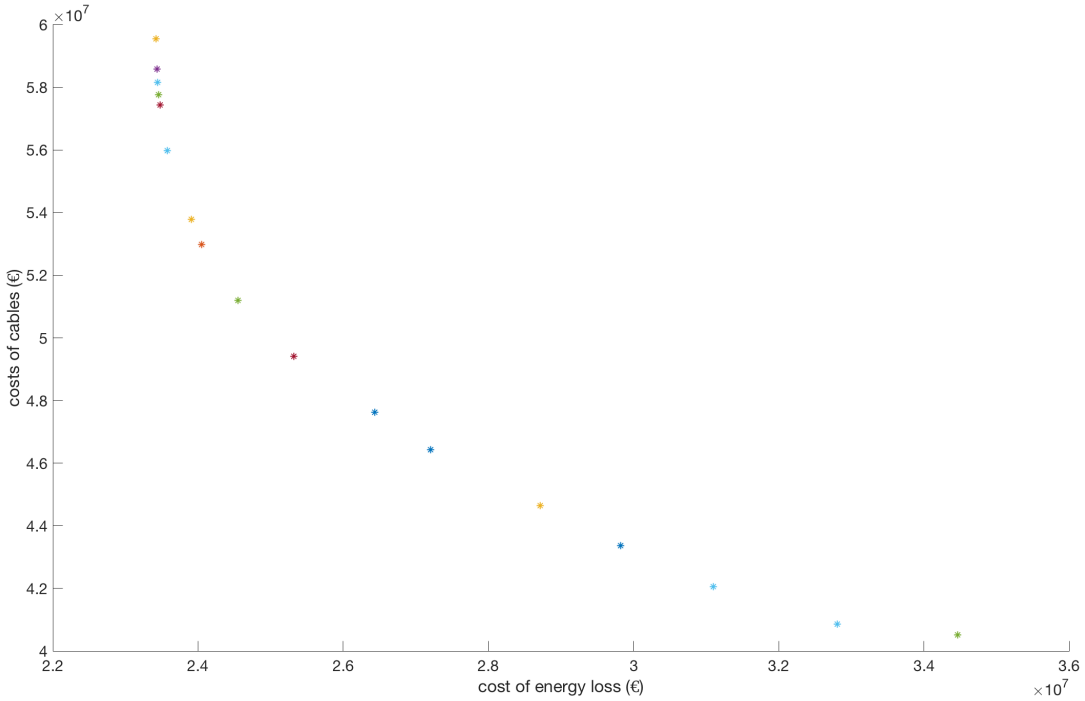

Figure 32: Pareto front of the multi-objective function of the third case study.

With the aim of surmising a range where the minimum can be achieved, the sum of the two costs without the weight factors, and only the combinations from the Pareto front, is plotted against the weight factor w_i of the multi-objective function in Figure 33. The lowest sum of costs is achieved for weights of 0.495 and 0.585 for w_1 with a sum of costs of 73.16 M€.

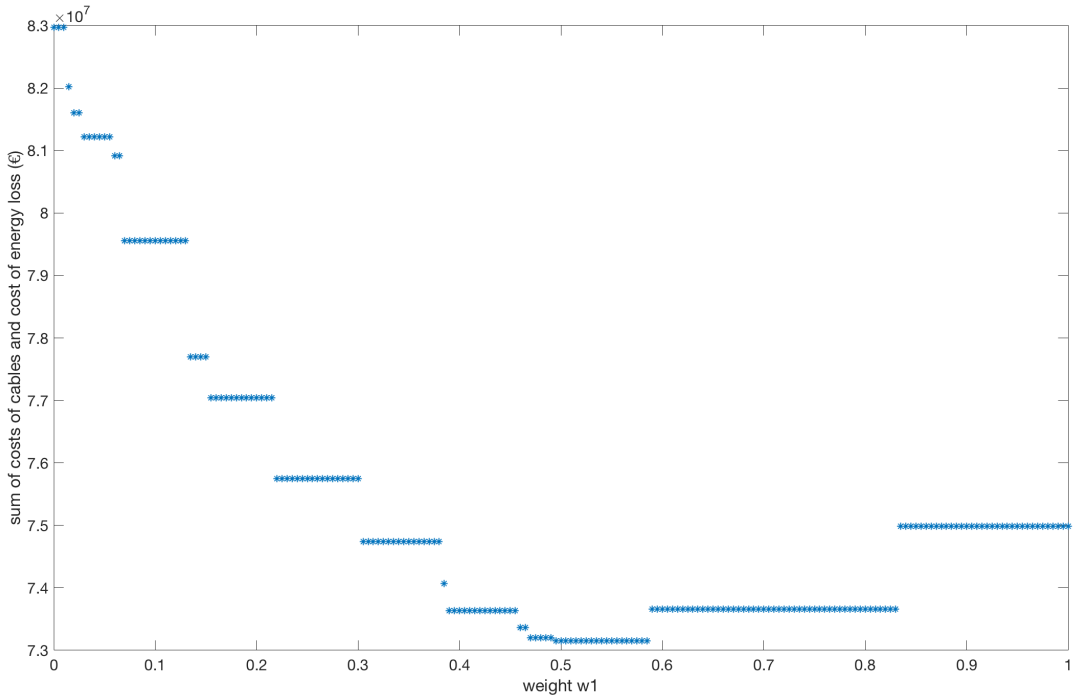

Figure 33: Sum of costs for each optimum depending on the weight factor for the third case study.

The wind farm layout with the optimized cable diameters is plotted in Figure 34, the cable combination is the same as in the second case since the number of wind turbines in a string-feeder has not changed. In the first and second section, from wind turbine 1 to wind turbine 3, the smallest diameter of 95 mm^2 is chosen, meanwhile for the following four sections, form wind turbine 3 to wind turbine 7, a diameter of 400 mm^2 and finally, for the lasts sections, from wind turbine 7 to the substation, a diameter of 800 mm^2 is designated.

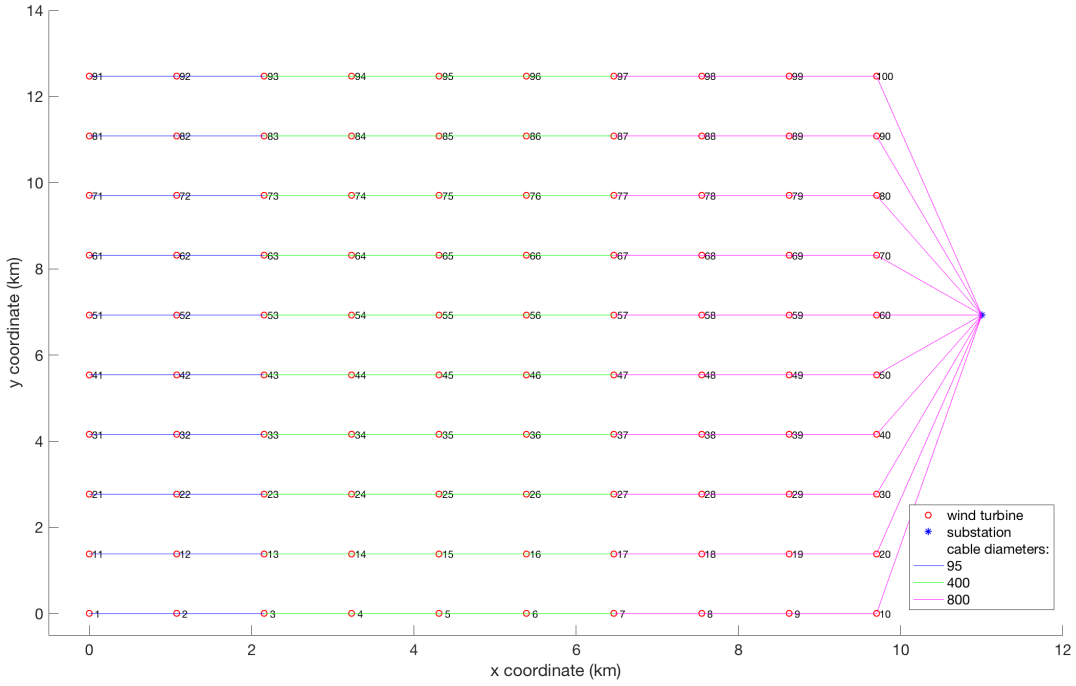

Figure 34: Optimized wind farm of the first case study: cable diameter and wind farm layout.

Set of cables	[95 400 800]
Total cost of cables	43.3737 M€
Relative power losses	0.8236%
Annual energy losses	15.8131 GWh
Total cost of energy losses	29.8229 M€
Sum of total costs	73.1966 M€
Total time to calculate all feasible solutions	2601.8918 seconds

Table 22: Results from the Optimized design of the third case study.

5.3.3 Discussion

The optimization implies a cable investment of 6.36 M€, which represents an increase of 17.19%. But, with a reduction on the relative power losses of 0.27% a decrease on the annual energy losses of 5.15 GWh or 24.56% is performed. The overall picture can be taken from the sum of both costs, considering the cost of energy loss as operational cost as well as the investment in cables, the Optimized design results in 3.34 M€on savings or a reduction of 4.37% of the investment required.

Design	Set of cables	Relative power losses (600 MW capacity)%	Annual energy losses GWh	Total cost of energy losses M€	Total cost of cables M€
Reference	95 120 185 240 400 500 630 800	1.09	20.96	39.53	37.01
Optimized	95 400 800	0.82	15.81	29.82	43.37

Table 23: Comparison of key values of the Reference and the Optimized design of the third case study.

Conclusions

Firstly a summary of the results is presented in order to draw conclusion for the different cases of study. Secondly the conclusions of the project and an outlook are presented.

Summary of results

The results of Cristoph's Research Assignment are compared to the First case study since the wind farm layout, number of wind turbines and cable length, and the OWPP capacity are the same but the rated voltage is different. As can be seen in Table 24 with the usage of array cables with a rated voltage of 45 kV, the number of different cable sections decreases leading to a reduction of the cables costs of nearly 6.13 M€for the Reference Design and 5.48 M€for the Optimized Design. The relative power losses decreases considerably implying a curtail in the total costs of energy losses of 3.24 M€for the Reference Design and 4.74 M€for the Optimized Design. Therefore, the upgrade on the rated voltage is recommended since it results in savings of the magnitude of 37.37 M€for the Reference Design and 10.22 M€for the Optimized Design.

Design	Set of cables	Relative power losses (294 MW capacity) %	Annual energy losses GWh	Total cost of energy losses M€	Total cost of cables M€
Cristoph Research Assignment (33 kV)					
Reference	95 120 185 300 500 800	1.1	10.47	19.75	20.13
Optimized	95 400 800	0.81	7.66	14.44	23.65
First Case Study (45 kV)					
Reference	95 120 185 240 400	0.93	8.76	16.51	≈ 14
Optimized	95 240 400	0.55	5.14	9.70	18.17

Table 24: Comparison key values for an OWPP capacity of 294 MW with different rated voltage.

The optimization on the Second case study leads into an increase of cable investment of 19.12% in comparison to the cable sizing method using the thermal rating. On the other hand, it also leads into a decrease of cost of energy losses of 27.08%. All in all, the optimization implies a reduction of the sum of both costs of 4.88%. Therefore, the aim of reducing both costs by the usage of the multi-objective optimization is achieved.

In order to get a more realistic survey, the Third case study is performed. With an OWPP capacity of 600 MW and 100 wind turbines represents one of the biggest offshore wind farms operating in the world right now. The optimization derives into an increase of cable investment of 17.19% in comparison to the cable sizing method using the thermal rating. By contrast, a decrease of the cost of energy losses of 24.56% is performed. In total, the optimization derives into a reduction of the sum of both costs of 4.37%. All things considered, the aim of reducing both costs by the usage of the multi-objective optimization is achieved.

Conclusions and Outlook

In this report an optimization for the array cables of an offshore wind farm is presented. Firstly, the theoretical background is explained. Following the optimization and the basis case are introduced. And finally three different case study are presented.

The main aim of the thesis is achieved for the different cases of study as can be seen in the previous section. Special attention should be paid into the First case, as it shows that the upgrade of the rated voltage is beneficial referring to the total investment required for the wiring of an offshore wind farm, since with a lower current a greater capacity is allowed and the power losses are reduced. Also, note that the Third case is the most realistic, since wind power is still in process of development, and it seems that the future will involve larger wind farms. In fact, recently the company *Iberdrola* announced the begging of the installation of the wind turbines on the East Anglia One, the biggest offshore wind farm project, which will be operative by 2020 with a capacity of 704 MW.

Therefore, it could be interesting to continue this work with bigger wind farms, new topologies or different array cables, and mostly, implementing this optimization to a real offshore wind farm since the future should involve more green ways of power generation in order to reduce the human impact on the planet, as the climate change.

In addition, further studies could address the wind distribution, different approach for calculation the energy losses adding the wake losses, and the study behind the compensation of the reactive power.

Acknowledgements

This thesis would not have been possible without the support of some people, who at some point guided and helped me throughout the process.

Special gratitude to Oriol Gomis, my director who proposed this topic following my directions, which were not few.

A very special thanks to Cristoph Kaufmann, for allowing me to try to continue his work and getting involved as well as helpful.

Thanks to Jovana for her willingness at any time.

And finally, a big thanks to my family and friends, for the constant support along the bachelor. Without your encouraging I do not know if I would be where and who I am today.

References

Articles

[1] Fatih Birol et al. "World energy outlook". In: *Paris: International Energy Agency* 23.4 (2008), p. 329.

[6] Rebecca Jane Barthelmie et al. "Modelling and measurements of power losses and turbulence intensity in wind turbine wakes at Middelgrunden offshore wind farm". In: *Wind Energy: An International Journal for Progress and Applications in Wind Power Conversion Technology* 10.6 (2007), pp. 517–528.

[9] Helen Bailey, Kate L Brookes, and Paul M Thompson. "Assessing environmental impacts of offshore wind farms: lessons learned and recommendations for the future". In: *Aquatic biosystems* 10.1 (2014), p. 8.

[11] International Renewable Energy Agency. "Innovation outlook: offshore wind." In: *IRENA's Renewable Energy Innovation Outlook* (2016), p. 160.

[12] N Barberis Negra, Jovan Todorovic, and Thomas Ackermann. "Loss evaluation of HVAC and HVDC transmission solutions for large offshore wind farms". In: *Electric power systems research* 76.11 (2006), pp. 916–927.

[17] Mikel de Prada Gil. "Design, operation and control of novel electrical concepts for offshore wind power plants". In: (2014).

[20] M Pavlovsky and P Bauer. "Cable selection and shunt compensation for offshore windparks". In: *Delf University of Technology* (2003).

[22] Nigel Hampton et al. "Long-life XLPE insulated power cable". In: (2007).

[25] S Lumbreras and A Ramos. "Offshore wind farm electrical design: a review". In: *Wind Energy* 16.3 (2013), pp. 459–473.

[26] Sara Lumbreras and Andres Ramos. "Optimal design of the electrical layout of an offshore wind farm applying decomposition strategies". In: *IEEE Transactions on Power Systems* 28.2 (2012), pp. 1434–1441.

[27] Athanasios Papadopoulos. "Modeling of collection and transmission losses of offshore wind farms for optimization purposes". In: (2015).

[28] Kevin Schönleber, Sergi Ratés-Palau, and Oriol Gomis-Bellmunt. "Analysis of reactive power strategies in HVDC-connected wind power plant clusters". In: *Wind Energy* 20.12 (2017), pp. 1971–1982. ISSN: 10991824. DOI: 10.1002/we.2134.

[31] George J Anders and Heinrich Brakelmann. "Improvement in cable rating calculations by consideration of dependence of losses on temperature". In: *IEEE Transactions on Power Delivery* 19.3 (2004), pp. 919–925.

[32] Goran Andersson. "Electric power systems". In: *ETH Zurich* 4.1 (2010), pp. 75–76. DOI: 10.1109/MIE.2010.936104.

[33] Jordi-Roger Riba. "Analysis of formulas to calculate the AC resistance of different conductors' configurations". In: *Electric Power Systems Research* 127 (2015), pp. 93–100.

[34] AAP Silva and JMB Bezerra. "Applicability and limitations of ampacity models for HTLS conductors". In: *Electric Power Systems Research* 93 (2012), pp. 61–66.

[35] WI Middleton and EW Davis. "Skin effect in large stranded conductors at low frequencies". In: *Journal of the American Institute of Electrical Engineers* 40.9 (1921), pp. 757–763.

[36] Vincent T Morgan. "The current distribution, resistance and internal inductance of linear power system conductors—a review of explicit equations". In: *IEEE Transactions on Power Delivery* 28.3 (2013), pp. 1252–1262.

[39] MM Al-Asadi et al. "A simple formula for calculating the frequency-dependent resistance of a round wire". In: *Microwave and Optical Technology Letters* 19.2 (1998), pp. 84–87.
[43] Kevin Schönleber et al. "Optimization-based reactive power control in HVDC-connected wind power plants". In: *Renewable energy* 109 (2017), pp. 500–509.
[44] Simon Catmull et al. "Cyclic load profiles for offshore wind farm cable rating". In: *IEEE Transactions on Power Delivery* 31.3 (2015), pp. 1242–1250.
[47] Antonio Colmenar-Santos et al. "Simplified analysis of the electric power losses for onshore wind farms considering weibull distribution parameters". In: *Energies* 7.11 (2014), pp. 6856–6885.
[51] Mohsen Sedighi et al. "Simultaneous optimization of electrical interconnection configuration and cable sizing in offshore wind farms". In: (2018). DOI: 10.1007/s40565-017-0366-0. URL: https://doi.org/10.1007/s40565-017-0366-0.
[52] Fei Duan. "Wind Energy Cost Analysis: CoE for offshore Wind and LCOE financial modeling". In: (2017).
[53] AC Pillai et al. "Offshore wind farm electrical cable layout optimization". In: *Engineering Optimization* 47.12 (2015), pp. 1689–1708.
[54] M Dicorato et al. "Guidelines for assessment of investment cost for offshore wind generation". In: *Renewable energy* 36.8 (2011), pp. 2043–2051.
[57] R Timothy Marler and Jasbir S Arora. "Survey of multi-objective optimization methods for engineering". In: *Structural and multidisciplinary optimization* 26.6 (2004), pp. 369–395.
[58] Nyoman Gunantara. "A review of multi-objective optimization: Methods and its applications". In: *Cogent Engineering* 5.1 (2018), p. 1502242.
[59] Jared L Cohon and David H Marks. "A review and evaluation of multiobjective programming techniques". In: *Water Resources Research* 11.2 (1975), pp. 208–220.
[60] Giorgio Chiandussi et al. "Comparison of multi-objective optimization methodologies for engineering applications". In: *Computers & Mathematics with Applications* 63.5 (2012), pp. 912–942.
[65] Mikel De Prada et al. "Hybrid AC-DC offshore wind power plant topology: optimal design". In: *IEEE Transactions on Power Systems* 30.4 (2015), pp. 1868–1876.

Books

[3] Oriol Gomis-Bellmunt Dirk Van Hertem and Jun Liang. *HVDC GRIDS for offshore and supergrid of the future*. A JOHN WILEY SONS, INC., PUBLICATION, 2015.
[29] Leonard L Grigsby. *Electric power generation, transmission, and distribution*. CRC press, 2018.
[42] G.F. Moore. *Electric Cables Handbook*. Blackwell Science, 1997.
[48] Arthur R Bergen. *Power systems analysis*. Pearson Education India, 2009.
[61] Matthias Ehrgott. *Multicriteria optimization*. Vol. 491. Springer Science & Business Media, 2005.
[63] Constantin Niculescu and Lars-Erik Persson. *Convex functions and their applications*. Springer, 2006.

Web pages

[2] IEA. *Market analysis and forecast from 2018 to 2023*. 2018. URL: https://www.iea.org/renewables2018/power/ (visited on 2018).

[4] American Geosciences Institute. *Advantages and disadvantages of offshore wind farms*. 2019. URL: https://www.americangeosciences.org/critical-issues/faq/what-are-advantages-and-disadvantages-offshore-wind-farms (visited on 2019).

[7] Wind Europe. *Why offshore wind is essential to the fight against climate change*. 2019. URL: https://windeurope.org/newsroom/news/why-offshore-wind-is-essential-to-the-fight-against-climate-change/ (visited on 2019).

[14] Rampion Offshore Wind Farm. *Offshore infrastructure*. URL: https://www.rampionoffshore.com/wind-farm/components/offshore-substation/.

[18] ABB. *XLPE Submarine Cable Systems Attachment to XLPE Land Cable Systems-User´s Guide Rev 5 2 XLPE Submarine Cable Systems | ABB*. URL: https://new.abb.com/docs/default-source/ewea-doc/xlpe-submarine-cable-systems-2gm5007.pdf.

[19] Edvard Csanyi. *Characteristics of XLPE insulated cables*. 2019. URL: https://electrical-engineering-portal.com/characteristics-of-xlpe-insulated-cables-with-reference-to-the-uk-standards (visited on 2019).

[21] Prysmain Group. *SUPPORTING THE DEVELOPMENT OF SMARTER AND GREENER POWER GRIDS*. 2012. URL: https://www.prysmiangroup.com/en/en_hv-and-submarine_submarine-energy-systems_hvac-submarine_submarine-energy-systems.html (visited on 2012).

[23] Universal Cable. *XLPE Insulated Power Cables*. URL: http://www.ucable.com.my/images/products/UC%20XLPE%20Catalogue.pdf.

[24] ABB. *XLPE Land Cable Systems, User's guide*. URL: https://library.e.abb.com/public/ab02245fb5b5ec41c12575c4004a76d0/XLPE%20Land%20Cable%20Systems%202GM5007GB%20rev%205.pdf.

[37] Keith Armstrong. *Skin Effect and Surface Currents*. 2018. URL: https://incompliancemag.com/article/skin-effect-and-surface-currents/.

[38] Circuit Globe. *Skin Effect*. URL: https://circuitglobe.com/skin-effect.html.

[49] Circuit Globe. *Per Unit System*. URL: https://circuitglobe.com/what-is-a-per-unit-system.html.

[66] Siemens Gamesa. *Offshore Wind Turbine SWT-6.0-154 I Siemens Gamesa*. 2014. URL: https://www.siemensgamesa.com/en-int/products-and-services/offshore/w%20ind-turbine-swt-6-0-154.

Others

[5] Tampere University of Technology Enrique Acha. "Lecture 1, Wind Power Systems". 2018.

[8] Luis Ignacio Candel Laveda. "Diseño e impacto ambiental de un parque eólico offshore". 2015.

[10] Cristoph Kaufmann. "Optimization of Cable Sizes of an Offshore Wind Farm Collector System using a Multi-objective Function". 2018.

[15] Tampere University of Technology Enrique Acha. "Lecture 2, Wind Power Systems". 2018.

[50] University of British Columbia. "The Newton-Raphson Method". 2019. URL: http://www.math.ubc.ca/~anstee/math104/newtonmethod.pdf.

[64] Politecnico di Milano Gianluca Palermo. "Introduction to Dynamic AutoTuning". 2018.

A Appendix: Voltage Check

The voltage drop at each wind turbine is obtained in order to check if exceeds the tolerance of 5%. Each red circle represents a wind turbine and from the y axis the value can be read, and so check of the voltage drop is higher than a 5 illustrated as *1.05* since the voltage is in the per-unit system. Therefore, following the graphs with the voltages are presented for each case study and each design.

A.1 First Case Study

The highest voltage of the wind turbines in the Reference Design is performed in wind turbine 1 with 1.67% above the reference voltage of the substation. And for the Optimized Design, is performed in the wind turbine 1 as well with 1.01% above the reference voltage of the substation.

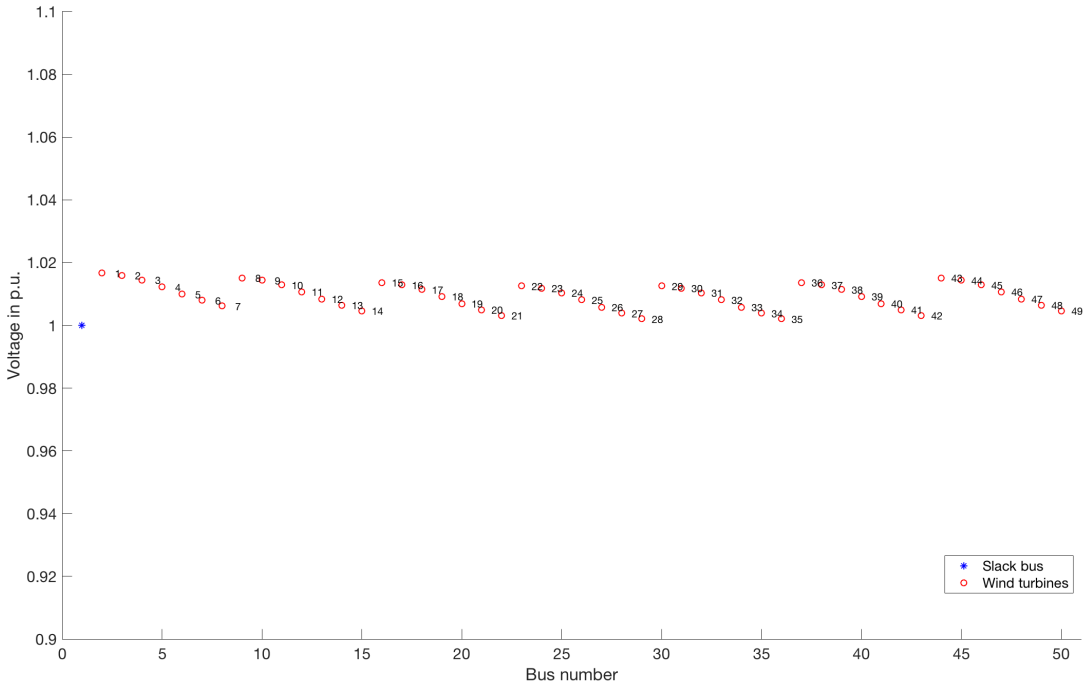

Figure 35: Reference wind farm of the first case study: voltages at each wind turbine.

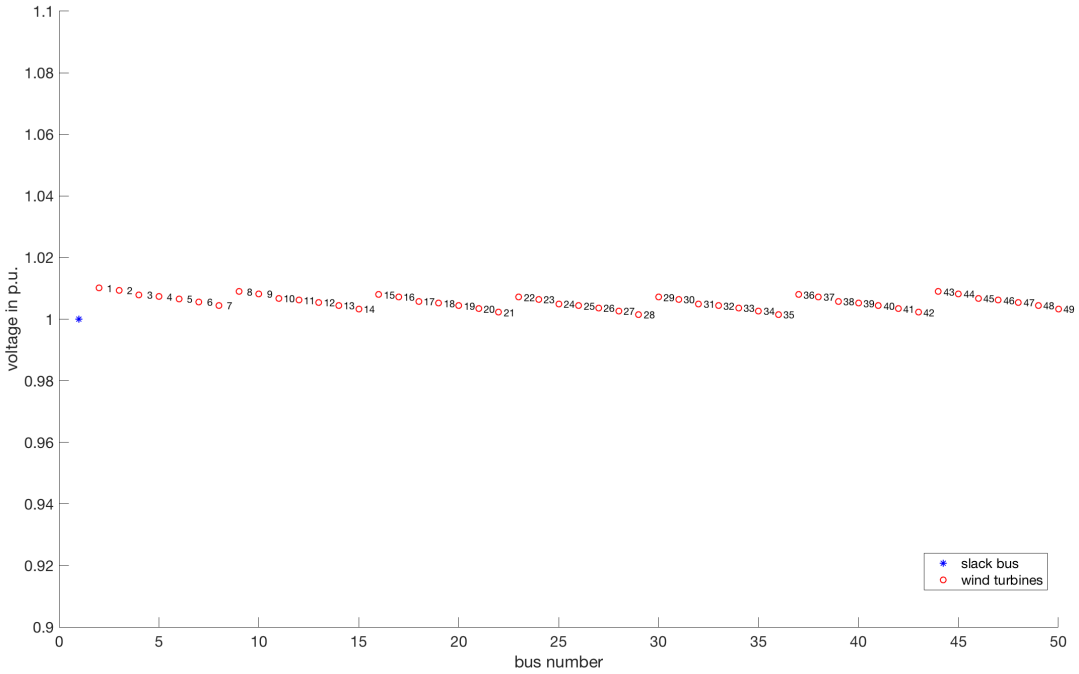

Figure 36: Optimized wind farm of the first case study: voltages at each wind turbine.

A.2 Second Case Study

The highest voltage of the wind turbines in the Reference Design is performed in wind turbine 1 with 1.67% above the reference voltage of the substation. And for the Optimized Design, is performed in the wind turbine 1 as well with 1.01% above the reference voltage of the substation.

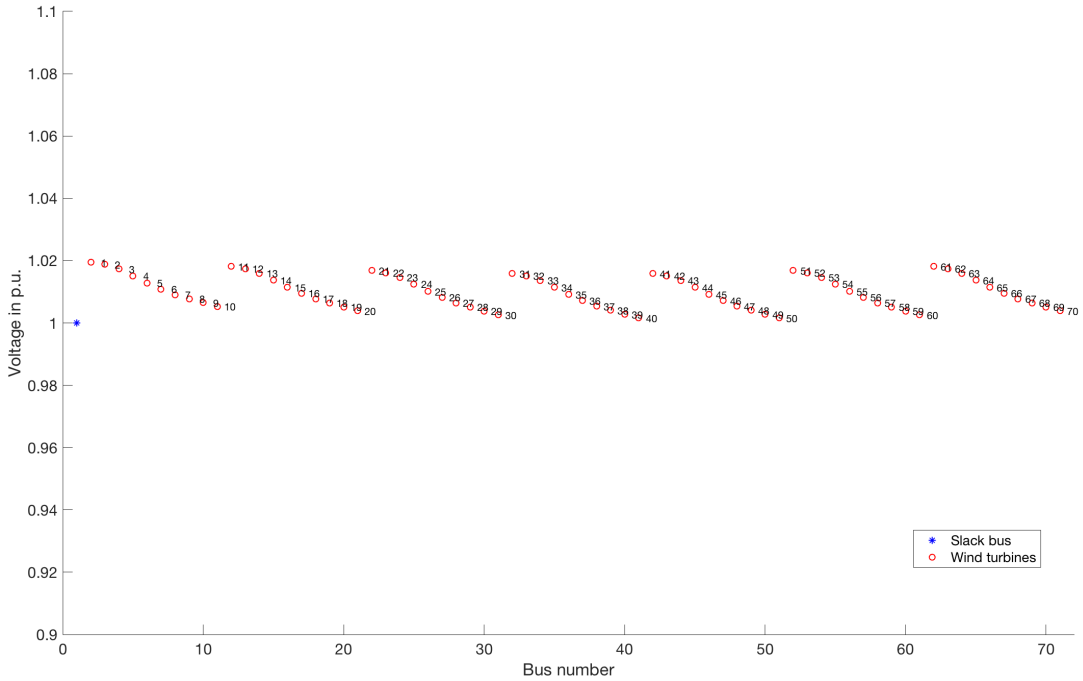

Figure 37: Reference wind farm of the second case study: voltages at each wind turbine.

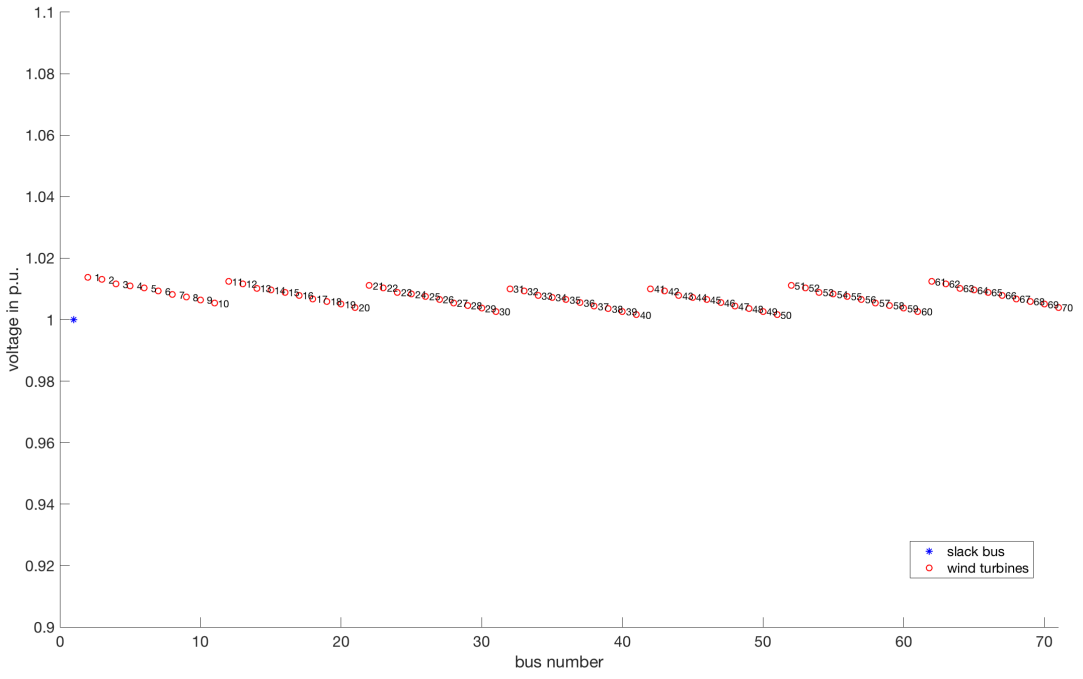

Figure 38: Optimized wind farm of the second case study: voltages at each wind turbine.

A.3 Third Case Study

The highest voltage of the wind turbines in the Reference Design is performed in wind turbine 1 with 2.15% above the reference voltage of the substation. And for the Optimized Design, is performed in the wind turbine 1 as well with 1.15% above the reference voltage of the substation.

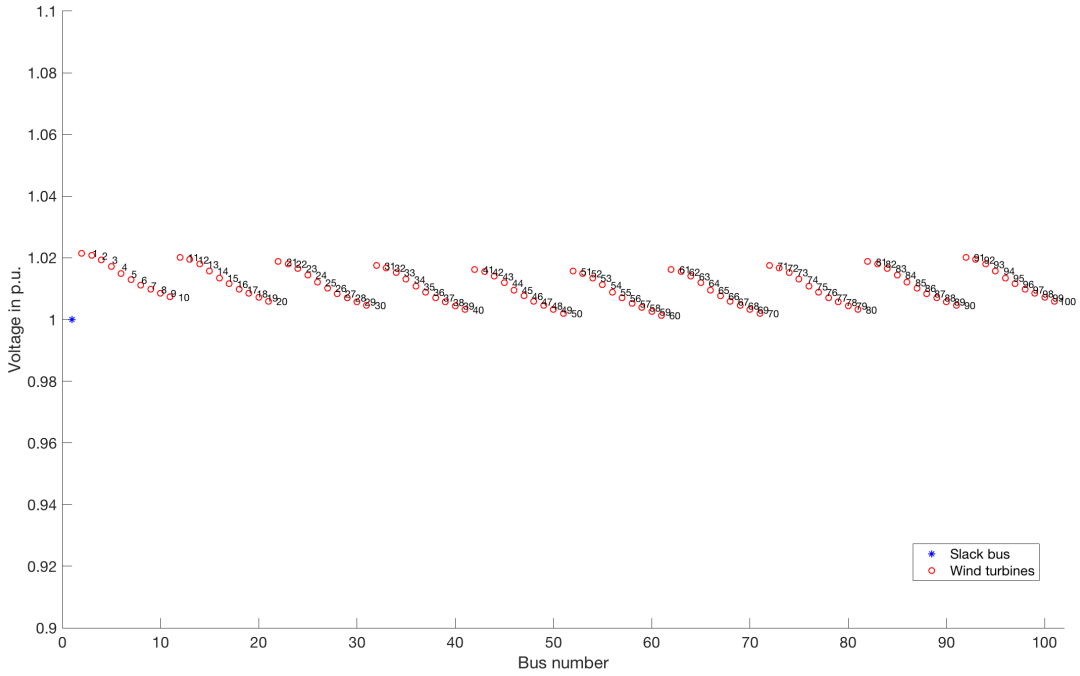

Figure 39: Reference wind farm of the third case study: voltages at each wind turbine.

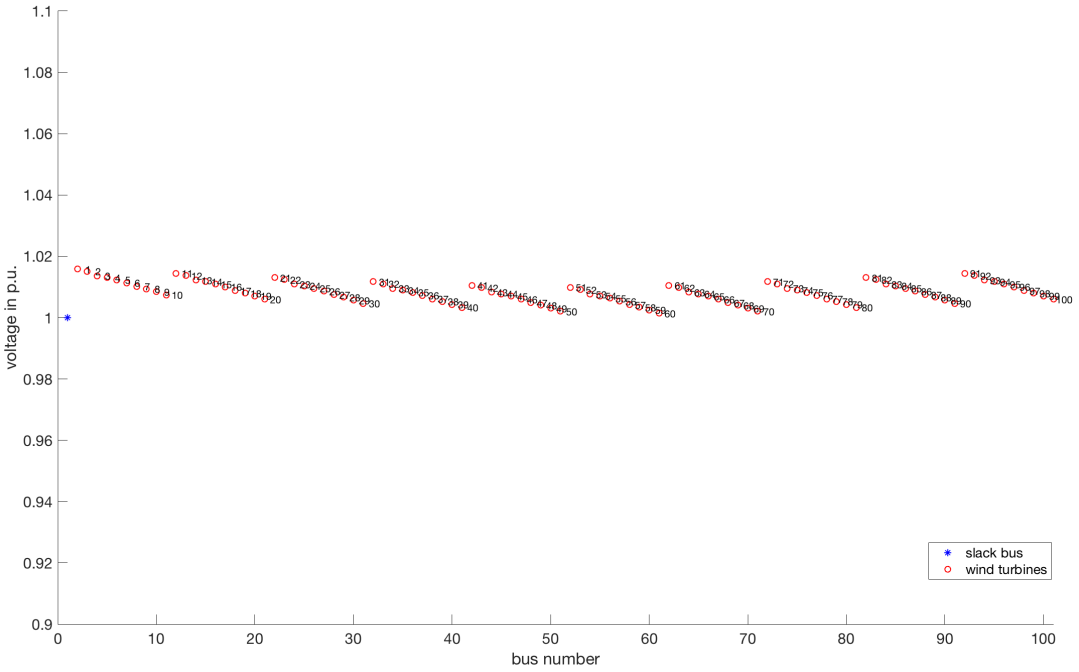

Figure 40: Optimized wind farm of the third case study: voltages at each wind turbine.

B Appendix: Environmental Impact

The environmental impact of an offshore wind farm is presented in this section. Several ambient characteristics are involved since the diversity of the study zone. The impact of the offshore wind farm is studied during the construction phase, operating phase and dismantling phase. Following, the impact on the biotic environment is presented. And latter the social-economic impact is explained.

B.1 Construction Phase

B.1.1 Geology

In the construction phase, the materials needed are deposited in a structure, which would affect the activity of a possible nearby harbour. The installation of the foundations of the wind turbines makes it necessary to remove large masses of land, although the impact will be greater or lesser depending on the type of foundation. The excavated lands, because of the foundations, depending on their disposition, could change the wave regime and currents, thus modifying the local morphology.

B.1.2 Alteration of the Seabed

The submarine cables that connect the wind turbines to the transformation center, require excavation of the ground to be buried, and thus, have less impact, but this would cause a sediment lift in the entire water column and death of benthic communities.

The platforms that are used and that are seated on the seabed have also an impact on the environment.

B.1.3 Seabed Pollution

Pollution can occur due to the spillage of fuels or oils from the vessels and machinery used.

B.1.4 Alteration of Water Quality

It can be caused by the excavation for foundations and power lines. The quality of the water will be affected by the excavation carried out on the seabed to bury the evacuation lines, which will cause a cloud of sediments. This sediment cloud will affect above all the benthic communities. In any case, it will be a temporary impact.

B.2 Operating Phase

B.2.1 Alteration of the Seabed

During the operation phase of the wind farm, there is a collapse of the structures in the terrain.

B.2.2 Seabed Pollution

The contamination may be due to the presence of the transformer substation (in case it is built on a platform in the sea) and to the possible accidents generated by the vessels carrying out the maintenance.

B.2.3 Airborne Noise

During the operation phase, there will be noises coming from the rotation of the blades and the internal mechanisms of the tower and the nacelle, causing vibrations in the marine and aerial environment. In the aerial environment it will have an impact on the birds and the population. The noise produced during the operation of the park can be decreased if the aerogenerators are kept in good condition. Wind speed will also affect.

In a study on a wind farm it has been seen that the noise made by wind turbine turbines is lower than that of passenger ships.

B.2.4 Air Quality

During the operation of the wind turbines there are no emissions to the atmosphere, therefore, wind energy represents a saving in greenhouse gas emissions compared to other traditional forms of electric power generation and would therefore be an impact positive about air quality.

B.2.5 Noise and Underwater Vibrations

The sound under water is generated by the vibrations of the tower. The towers, having a large contact surface with the water, will transmit the sound with great efficiency. The tower will also transmit vibrations to the bottom of the sea, but these are considered irrelevant. In the air, the blades, although they are on the surface of the water, will not affect the sound level under water.

B.2.6 Electric Field

The electrical wiring will generate an electric and magnetic field around it, which will affect marine mammals that use the earth's magnetic field to travel. Also, they can cause errors in the navigation instruments of the boats.

B.2.7 Alteration of Water Quality

The alteration can be due to:

- The excavation for foundations and power lines.
- Release of copper from wind turbines.

B.3 Dismantling Phase

B.3.1 Geology

In the dismantling phase, the affected area could be expanded, since it is necessary to remove the soil in order to raise the entire structure. This also depends on the technique used in the removal.

The materials of the foundations can be reused for the construction of roads or as an addition to concrete. Also the steel of the turbines can be reused.

B.3.2 Seabed Pollution

Pollution can occur due to the spillage of fuels or oils from the vessels and machinery used.

B.4 Biotic Environment Impact

B.4.1 Birds

One of the main concerns surrounding offshore wind farms is the risk of collision with wind turbines, which can lead to high bird mortality rates. Most of the birds at risk are seabirds.

Although there is much literature on the potential effects that offshore wind farms have on birds, the consequences of construction and operation are common and include:

- Constitution of a barrier to the movement of birds.
- Displacement of their usual areas.
- Adverse effects on the areas and sources of food.
- Risks of collision with the wind turbines.

B.4.2 Benthic Fauna

The greatest impact on the benthic fauna occurs during the construction and dismantling phase. The turbidity generated in this phases can temporarily affect the primary producers, which represents a loss for the fish as a source of food.

The most common impacts are:

- Loss of habitats and individuals due to construction activities. However, disturbances of the sediments during this phase are only temporary.
- The change in the currents around the turbine, can move the sediments of immediately around, as well as the cables. Electromagnetic radiation and noise can disturb life on the seabed.
- The bases act as natural reefs, however, this hard artificial substrate can cause changes in the biotope with unknown consequences on the benthos and later on the food chain.
- The absence of fishing and maritime transport (except for maintenance vessels) will have a positive effect on the local fauna and the seabed.

B.4.3 Fishes

Offshore wind farms can influence fish communities during all phases of the farm's existence. The main effects associated during the construction only take place during short periods of time and no long-term effects are derived. However, two elements do have long-term effects: the establishment of turbines, which create a new habitat, and the transmission of electricity to the ground, which generates a weak electromagnetic field along the cable that can be captured for some species of fish.

B.4.4 Sea Mammals

Marine mammals can be affected in several ways. During the construction phase, the noise and vibrations of the assembly and other works exclude these animals at a great distance. During the operation phase, the sound and vibration are still emitted to the water and make communication difficult and modify the behavior of the animals.

In general, these animals use underwater sound for functions such as communication, location and characterization of prey, orientation and avoidance of predators.

B.4.5 Flora

The effects on the flora can lead to the creation of new habitats or alteration or elimination of them. In most offshore wind farms, the presence of wind turbines has not meant a great change in the flora of the area. The presence of wind turbines causes changes in marine currents, which

would lead to modify the communities of organisms settled in that habitat. Depending on the form of anchorage of the wind turbines, there will be different species.

B.5 Social-Economic Impact

A key point for the development of an offshore wind farm installation project is to determine the effect that this facility may have in the population as well as the possible impacts it may generate in the economy, since the convenience of the investment depends on that.

B.5.1 Conflict of Uses

- Risk of collision of ships and ships and effects on maritime navigation and commercial fishing.
- Effects on military activities.
- Effects in aviation and telecommunications.
- Noise.
- Effects in places of archaeological importance.

B.5.2 Visual Impact

The visual impact of wind turbines is one of the main problems with offshore wind power.

In addition to that, during the construction phase, the presence of boats, equipment and cranes, can cause some turbidity to the waters.

B.5.3 Social Impacts

Social acceptance is a key aspect when dealing with the deployment of offshore wind power. It can have effects on:

- The tourism.
- The population.
- The economy.

C Appendix: Budget

This thesis is composed of two sections, research and development. In order to develop these two parts, office hardware, office software and human resources are valued in different budget sections.

C.1 Office Hardware

A computer is needed to conduct the research, develop the wind farm designs and optimizations, as well as to write this thesis. Since it is expected to use the computer in the future, only a 15 % of the total cost will be taken into account.

Concept	Unitary price	Units	Total
MacBook Pro.	1,449.00 €	0.15	217.35 €
Total			217.35 €

Table 25: Office hardware budget.

C.2 Office Software

In order to run the simulations, the The MathWorks Inc. software Matlab® is needed, as well as Microsoft Excel to analyze the results. Overleaf is the software used to write the report, with half price for students.

Concept	Unitary price	Units	Total
Matlab® perpetual license	2,000.00€	1	2,000.00€
Microsoft Excel 2019	135.00 €	1	135.00 €
Overleaf, Online latex editor	7.00 €/month	5	35.00 €
Total			2,170.00 €

Table 26: Office software budget.

C.3 Human Resources

Human resources costs are divided in research hours, development hours and writing hours, assuming a salary of a junior researcher at 35 €/h and 30€/h for writing.

Concept	Unitary price	Hours	Total
Research	35.00€/h	250	8,750.00€
Development	35.00€/h	100	3,500.00€
Writing	30.00€/h	170	5,100.00€
Total			17,350.00 €

Table 27: Human resources budget.

C.4 Total Budget

The total budget is set by the sum of the former budgets, with a total of 20934 €.

Concept	Total
Office Hardware	217.35 €
Office Software	2,170.00 €
Human Resources	17,350.00 €
Total	19,737.35 €

Table 28: Total project budget.